Cocagne Bay 2014 Topo-Bathymetric Lidar Mapping Report

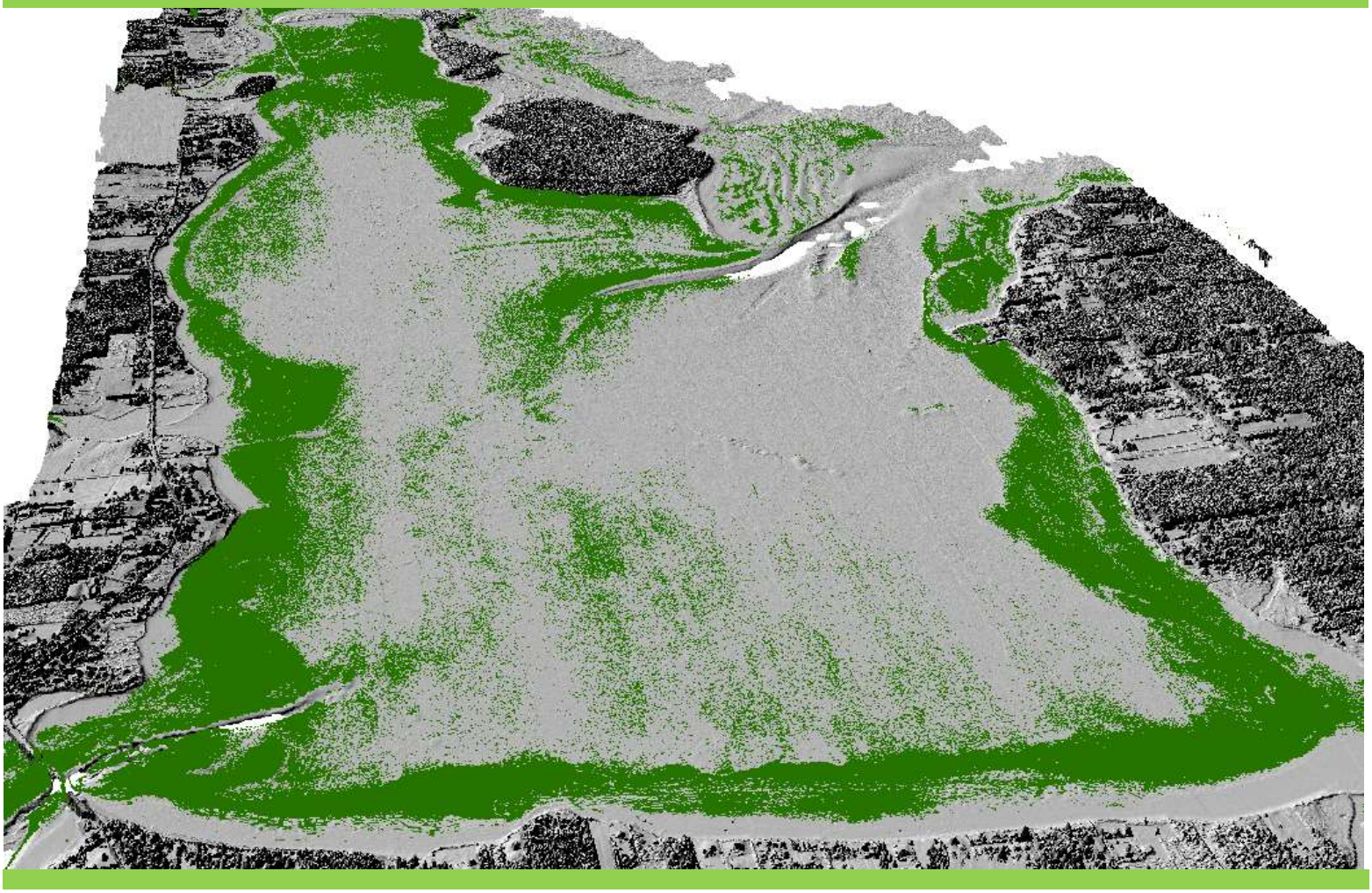

Prepared by

Tim Webster, PhD
Kevin McGuigan, Kate Collins, Nathan Crowell, Candace MacDonald
Applied Geomatics Research Group
NSCC, Middleton and
Matt Roscoe, DFO Gulf Region
Tel. 902 825 5475
email: tim.webster@nscc.ca

Submitted to

Marc Ouellette
Fisheries and Oceans
Maritimes Region

March, 2015

How to cite this work and report:

Webster, T., McGuigan, K., Collins, K.,Crowell, N., MacDonald, C., and Roscoe, M. 2014. Cocagne Bay 2014 Topo-Bathymetric Lidar Mapping Report. Technical report, Applied Geomatics Research Group, NSCC Middleton, NS.

Executive Summary

An airborne topo-bathymetric lidar survey was undertaken at Cocagne Bay, New Brunswick on September 25 and 26, 2014. The sensor used was a Chiroptera II integrated topographic bathymetric lidar sensor equipped with a 60 megapixel multispectral camera. Strong winds along the Northumberland Strait during the week of the planned survey reduced water clarity. The winds tended to be the strongest during the early afternoon and die down during the evening and night. As a result of these conditions and the size of the Cocagne Bay study area, it was surveyed over two days. The survey on Sept. 25 was conducted in the late afternoon and the survey on the 26th was conducted in the morning ensuring the clearest water conditions during that period. The aircraft required ground-based high precision GPS data from a NB High Precision Network (HPN) monument for both days (25th and 26th). Boat-based ground truth data collection was acquired by scientists from the Gulf Region of Department of Fisheries and Oceans near the time of the survey. The lidar data were processed in Lidar Survey Studio, a proprietary software that accompanies the Chiroptera II sensor, and classed into ground (includes trees and buildings), water surface, and bathymetric points that were used to produce a Digital Elevation Model (DEM) for the study area. Maps of lidar intensity data were also produced; these show information on the seabed cover type. The lidar sensor was also equipped with a Leica RCD 30 camera capable of collecting imagery for true colour (RGB) and near-infrared bands that were processed to orthophotos and mosaics constructed. These data were processed further to map out the 1 m depth intervals within the bay based on the lidar DEM, a calculation of oyster biomass based on the aquaculture infrastructure interpreted from the orthophotos as well as the spatial distribution of the cages, and finally an eelgrass distribution map derived from a combination of lidar and orthophoto data. The distribution of eelgrass for each depth interval was then calculated using GIS spatial analysis tools.

Table of Contents

Table of Figures

List of Tables

1 Introduction

The requirement for accurate and detailed information along Canada's coastal zone is imperative in order to protect existing and plan for future infrastructure, and to make sound decisions with regard to activities that support economic development. Recently the Applied Geomatics Research Group (AGRG) at the Nova Scotia Community College (NSCC) acquired a topographic-bathymetric (topo-bathy) lidar sensor and high resolution aerial camera that is capable of surveying the land elevations and the submerged coastal topography. The ability of an airborne sensor to accurately survey the near shore bathymetry (submerged elevation) offers an opportunity to produce detailed information across the land-sea boundary in an area that has traditionally not been mapped because of the expense and limitations of traditional mapping technologies (air photos on land and boats and echo sounders on the water).

The lidar system utilizes lasers mounted in an aircraft to precisely measure the topography surrounding coastal waters and also sees through the water to measure the bathymetry. The reflection of the green laser from the seabed can be used to also map the seabed cover including submerged vegetation, for example eelgrass, which is often used by regulators, such as Fisheries and Oceans Canada (DFO), as a measure of ecosystem health. These data can be used to capture the state of the seabed and aquatic vegetation and act as a quantitative baseline prior to any future coastal developments. The lidar sensor is coupled with a high resolution aerial camera (Leica RCD30) which is capable of collecting traditional true colour images (red, green, and blue or RGB) and also a near-infrared (NIR) image which is highly sensitive to the existence of vegetation, such as exposed seaweed in the coastal zone. The ability of the lidar sensor to acquire detailed elevation data on land and continuously into the submarine environment provides information that can be used, for the land areas, to assess risk of coastal flooding, erosion and geohazards. For the intertidal and sub tidal areas this level of information has never been surveyed and provides details for updates for navigation to accurately map the channel for safe passage for small craft harbours.

The Cocagne Bay study area (Figure 1) was surveyed on September 25 in the afternoon and September 26, 2014 in the morning. The survey was funded by DFO Gulf Region with various deliverables:

1. A 3-D point cloud of all the lidar returns (landward vegetation, buildings, wharves, ground, land-water interface, sea surface, and seabed)
2. A continuous Digital Elevation Model (DEM) from land to the submerged seabed
3. A continuous Digital Surface Model (includes trees, buildings, wharves etc.) from land to the submerged seabed
4. True colour and NIR orthophotos of the land and coastal zone
5. Lidar reflectance map of the seabed cover type (ie. eelgrass)

Eelgrass is often used by regulators, such as DFO, as a measure of ecosystem health, but an efficient method of mapping eelgrass is required to enable eelgrass to be monitored through time. Bathymetric lidar provides the opportunity to conduct repeat surveys to map the changes in both bathymetry and potentially the distribution of eelgrass over time.

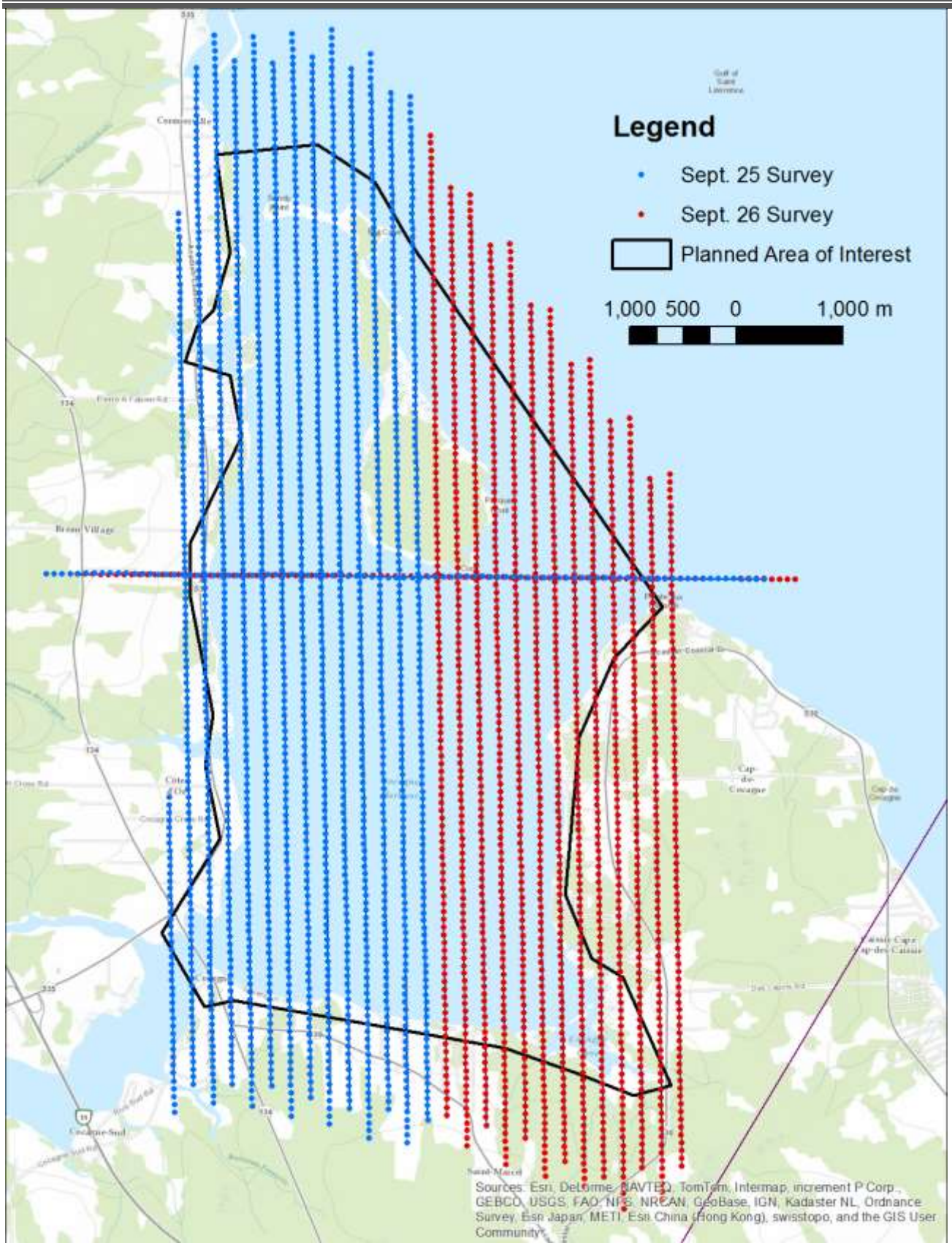

Figure 1: The study area for Cocagne Bay is defined by the heavy black line with the surveyed flight lines and camera exposures collected on Sept. 25 (blue dots) and 26th (red dots).

This report provides details on the instrumentation and processing in the Methods section, including details on the Chiroptera II lidar sensor used for the surveys (Section 2.1), the data processing methods (Section 2.4), the digitizing of aquaculture (Section 2.5), and the mapping of eelgrass (Section 2.6). The Results section includes maps of bathymetry, reflectance, and the orthophotos as well as aquaculture biomass estimates and eelgrass presence maps. Discussions & Conclusions contains evidence supporting the effect of aquaculture on eelgrass. The calibration report is provided in Appendix 1.

In addition to the initial data products from this sensor, this report also highlights deriving maps that are specific to the Program for Aquaculture Regulatory Research (PARR) project "The effect of cultured filter feeders on eelgrass productivity, in estuaries of NB and PEI" lead by Marc Ouellette of the Science Branch at DFO Gulf Region. Carr et al (2010) described a one-dimensional hydrodynamic model of vegetation-sediment-water flow interactions and used it to investigate the strengths of positive feedbacks between seagrass cover, stabilization of bed sediments, turbidity of the water column, and the existence of a favorable light environment for seagrasses in a shallow lagoon on the eastern shore of Virginia. The results indicate that under typical conditions, seagrass is stable in water depths < 2.2 m (51% of the bay bottom deep enough for seagrass growth) and bistable conditions exist for depths of 2.2–3.6 m (23% of bay) where the preferred state depends on initial seagrass cover. The remaining 26% of the bay is too deep to sustain seagrass. Decreases in sediment size and increases in water temperature and degree of eutrophication shift the bistable range to shallower depths, with more of the bay bottom unable to sustain seagrass. While others like Valle et al. (2011) used bathymetric lidar to model suitable habitats for eelgrass in northern Spain. Their objectives were to determine the main environmental variables explaining Zostera noltii distribution; to model habitat suitability for this species, as a wider applicable management-decision tool for seagrass restoration; and to assess the applicability and predicted accuracy of the model by using internal and external validation methods. They used the Ecological Niche Factor Analysis (ENFA) to model habitat suitability, based upon topographical variables, obtained from bathymetric lidar; sediment characteristics variables; and hydrodynamic variables. Their results indicate the main environmental variables relating to the species distribution, in order of importance, are: mean grain size; redox potential; intertidal height; sediment sorting; slope of intertidal flat; percentage of gravels; and percentage of organic matter content. In this project we plan to investigate the potential positive impact of filter feeding organisms on water clarity, which in turn effects the availability of light for eelgrass at a given depth to grow. Inputs into our analysis required the distribution of eelgrass which was obtained through processing the lidar and orthophotos, the distribution of suitable depth intervals, 1 m depths in our case, and the location and amount of filter feeder biomass, oyster aquaculture which was estimated from the infrastructure visible from the orthophotos.

2 Methods

2.1 Sensor Specifications and Installation

The lidar sensor is a Chiroptera II integrated topographic bathymetric lidar sensor equipped with a 60 megapixel multispectral camera. The system incorporates a 1064 nm near infrared laser for topographic (topo) laser for ground returns and a green 532 nm laser for hydrographic (hydro) returns (Figure 2). The lasers utilize a Palmer scanner, which forms an elliptical pattern with angles of incidence of 14^{o} forward and back and 20^{o} to the sides of the flight track. This enables more returns, lidar coverage from many different angles, on vertical faces, causes less shadow effects in the data, and is less sensitive to ocean wave interaction. The beam divergence of the topo laser is 0.5 mrad and from the hydro laser (green) is 3 mrad. The topo laser can scan with a pulse repetition frequency up to 400 kHz and the hydro laser can scan with a pulse repetition frequency up to 35 kHz. The hydro laser is limited by depth and water clarity, and has a depth penetration rating of approximately 1.5 x the Secchi depth (a measure of turbidity or water clarity). The Leica RCD30 camera collects co-aligned RGB+NIR motion compensated photographs which can be orthorectified and mosaicked into a single image in post-processing, or analyzed frame by frame for maximum information extraction. The RCD30 is a 60MPIX camera with a focal length lens of 53 mm and produces images 6732 by 9000 pixels in the across and along track direction, respectively. The across track field of view is 54^{o}.

AGRG-NSCC does not own an aircraft, only the sensor. AGRG partnered with Leading Edge Geomatics to assist in the operations of the survey and arranging the aircraft. A twin engine aircraft was contracted that was certified to carry the Chiroptera II sensor suite and had a hole suitable to house the sensor head. The lidar sensor was installed in the aircraft in Fredericton, NB on Sept. 22. Calibration flights were conducted over Fredericton at altitudes of 400 m and 100 m on Sept. 23. The laser systems and camera were calibrated and aligned with the navigation system which consists of a survey grade GPS mounted on the roof of the aircraft and an inertial measurement unit (IMU) mounted above the laser system (Figure 3). A report of the calibration procedure and results is supplied in

Appendix 1 Calibration Report of the Topo-Bathymetric lidar.

The aircraft has a hole cut in the bottom for the laser to face the ground and installation involves fitting the control unit and the sensor head into the hole (Figure 3b). The system also includes a 5 megapixel quality assurance camera that the lidar operator is able to view during the flight, along with the waveform of the returning pulse and the flight plan (Figure 3c). The exposure locations of the 5 MPIX camera are shown on Figure 1 to demonstrate the coverage on sept. 25 and 26th. Figure 3d shows the downward facing portion of the sensor head, including the red (topographic) and green (bathymetric) lasers, which shoot and return to the large red circles; the lenses on the left and right are the low and high resolution cameras, respectively.

The sensors were installed in the aircraft on Monday, September 22 (Figure 3a). The aircraft had a hole cut in the bottom for the laser and cameras to image the ground and installation involved fitting the sensor head into the hole (Figure 3c) and the associated control rack on the floor and user display screens on another rack in the aircraft (Figure 3b). Along with the lasers and high resolution camera, the lidar system also includes a 5 megapixel quality assurance camera that the lidar

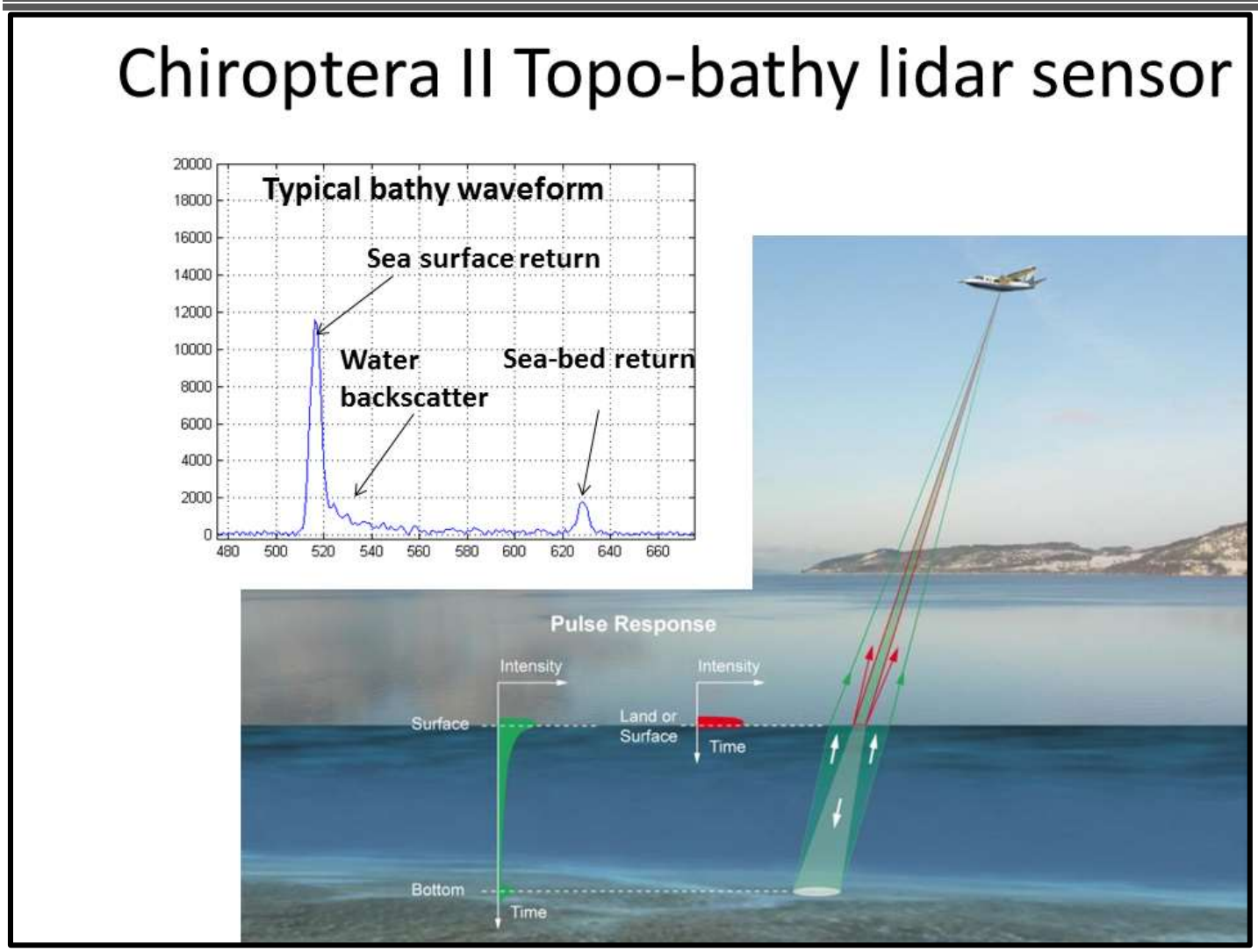

Figure 2 Principals of topo-bathymetric lidar. The system utilizes two lasers, a near infrared and a green laser to surface the land and marine topography.

Figure 3: (a) Aircraft used for September 2014 lidar survey; (b) display seen by lidar operator in-flight; (c) main body of sensor (left) and laser pointing through a hole cut in the bottom of the plane (right); (d) large red circles are the lasers; the RCD30 lens (right) and low resolution camera (left).

operator is able to view during the flight, along with the waveform of the returning pulse and the flight plan (Figure 3b). Figure 3d shows the downward facing portion of the sensor head, including the red (topographic) and green (bathymetric) lasers, which shoot and return to the large red circles; the lenses on the left and right are the low and high resolution cameras, respectively. During installation the laser systems and camera were calibrated and aligned with the navigation system which consists of a survey grade GPS mounted on the roof of the aircraft and an inertial measurement unit (IMU) mounted above the laser system. Calibration flights were conducted over Fredericton at altitudes of 400 m and 1000 m on Tuesday, Sept. 23, following a wind and rain event on Sept. 22.

2.2 Lidar Survey Details

A lidar survey was conducted for Cocagne Bay on Thursday afternoon September 25 and Friday morning September 26. Low tide at Cocagne Bay was predicted to occur at 18:04 ADT on Sept. 25 at a level of 0.72 m above local chart datum and at 6:01 ADT on Sept 26 at a level of 0.51 m above chart datum. The survey was planned using Mission Pro software at an altitude of 400 m above ground at a flying speed of 140 knots. The planned flight lines and photo events and photo footprints from the RCD30 are shown in Figure 4.

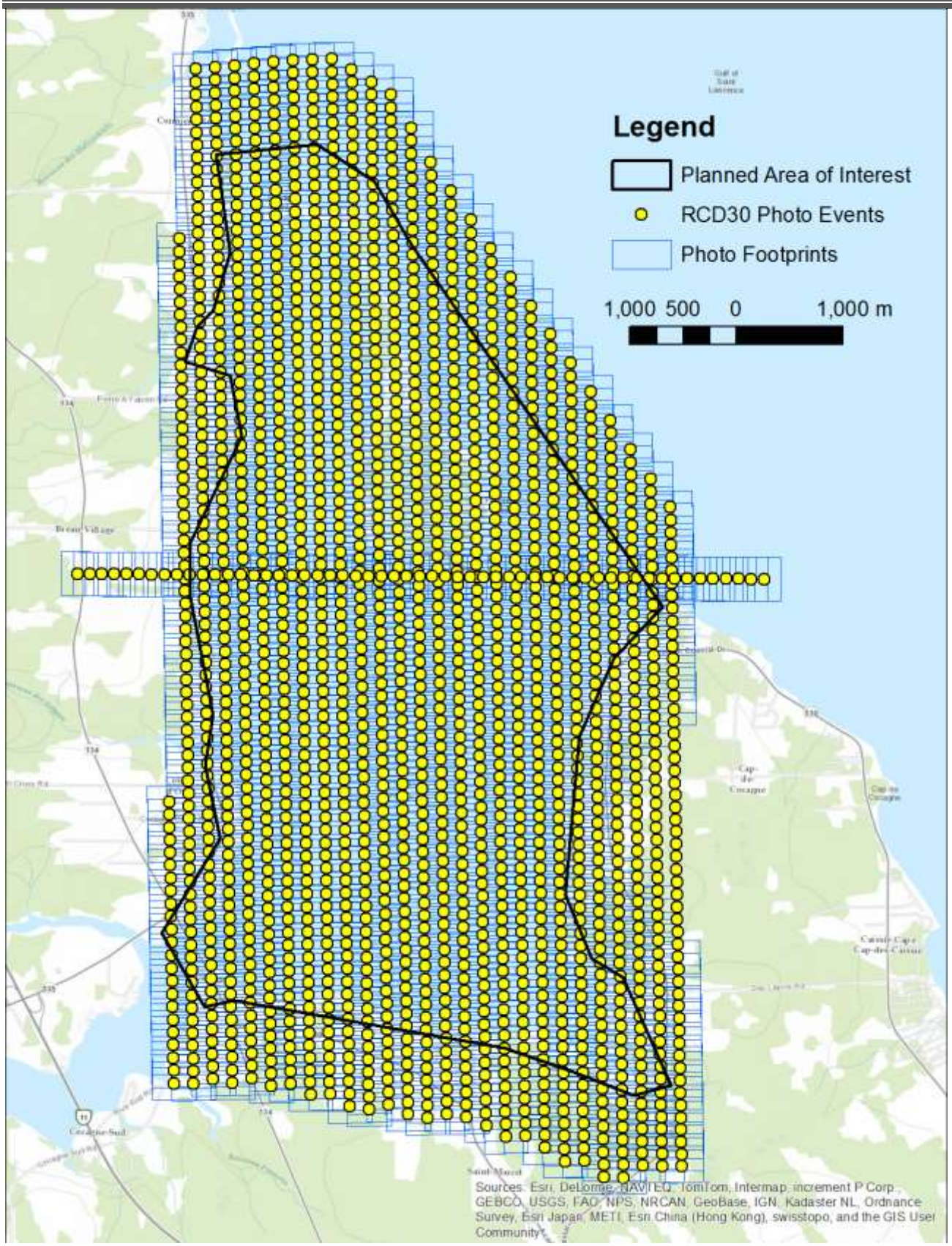

Figure 4 Planned flight lines and RCD30 photo camera events (yellow dots) with ground footprints (blue rectangles).

A NB High Precision Network (HPN) monument was used to establish a GPS base station for control of the aircraft trajectory and to collect Real Time Kinematic (RTK) GPS checkpoints to compare to the lidar DEM. The coordinates for HPN 8650 were acquired from Service New Brunswick and used for the base station (Figure 5) (Table 1).

Table 1 Coordinates for HPN 8650 from Service NB for GPS control.

Latitude (NAD83)	Longitude (NAD83)	Elevation m (Ellipsoidal)
46° 21’ 20.85229” N	64° 32’ 11.60203” W	-12.7897

Figure 5 NB HPN 8650 used for Cocagne Bay aerial survey and RTK GPS checkpoint collection GPS base station.

The GPS base station was set to log observations at 1 second intervals and the RTK rover was used to collect lidar validation points on hard flat surfaces (Figure 6). The survey area was constrained to the coastal areas so there were limited roads that could be used to collect GPS check points to be used for validation (Figure 6).

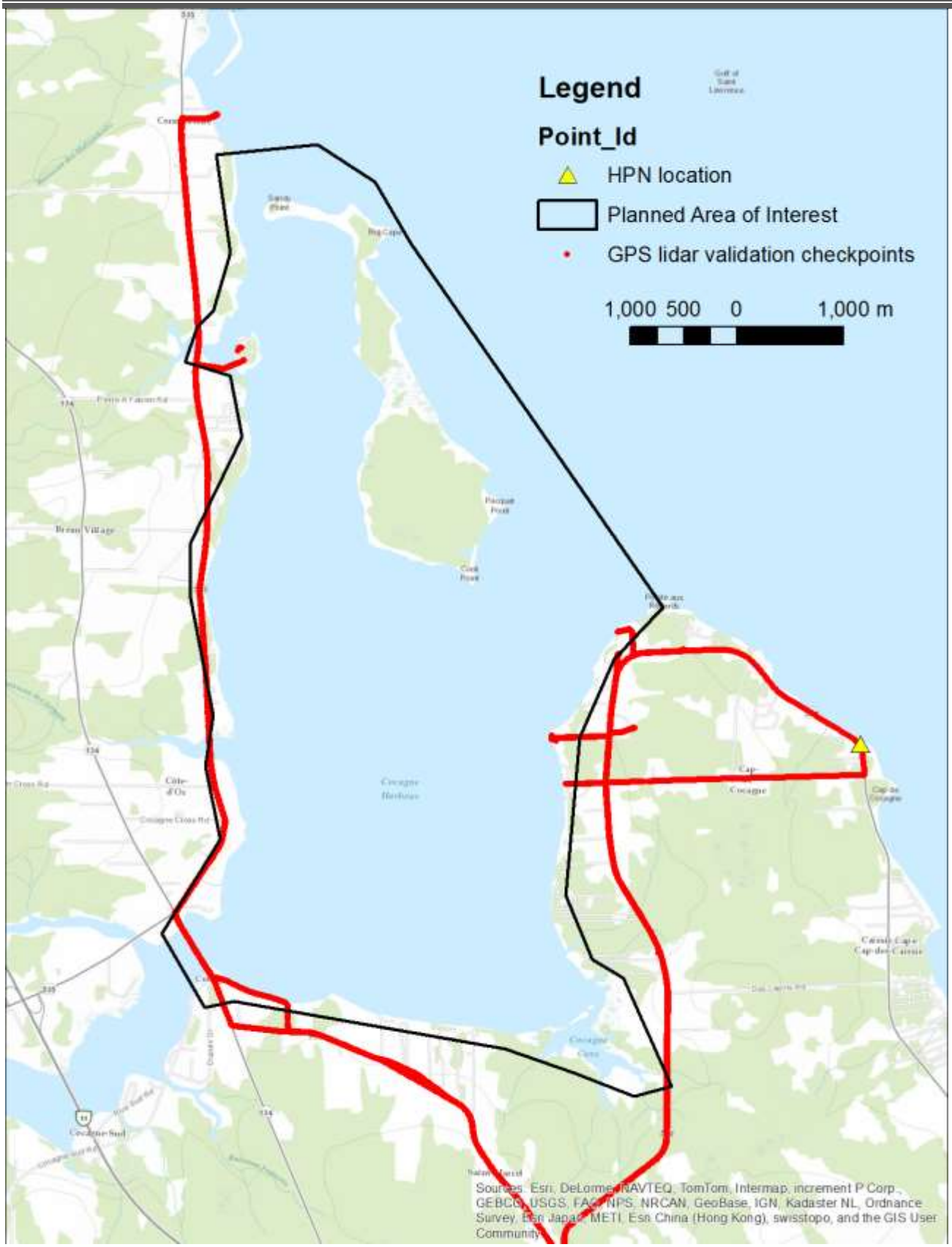

Figure 6 GPS base setup over NB HPN (yellow triangle) and GPS checkpoints collected from a vehicle for hard surfaces like roads (red points).

2.3 Meteorological Conditions

Meteorological conditions during and prior to topo-bathy lidar data collection are an important factor in successful data collection. As the lidar sensor is limited by water clarity, windy weather that stirs up sediment in the seawater can prevent good laser penetration. Rainy weather is not suitable for lidar collection, and the glare of the sun must also be factored in for the collection of aerial photography. The closest weather station to the site is operated by Environment Canada at Moncton, NB. In addition to checking the current and past conditions, local knowledge of the water clarity is critical. We were assisted by a local person, Brandan McKeil from the Cape Cocagne Marina, who provided us with information on the water clarity and wind conditions.

Figure 7 shows wind data recorded at Moncton in the days before and during the survey and shows a strong north-easterly wind event on Sept. 23. The wind speed slowed and rotated to the south on the 24th, then back to the north on the 25th to less than 30 km/hr. Prior to this it was reported that the water in the bay was extremely turbid and the bottom could not be seen visually. Eventually the winds died down during the night of the 24th, and this gave the water in the bay enough time to clear. The wind on the 25th were below 20 km/hr and from the southeast, thus the western side of Cocagne Bay was calm but got progressively rougher to the east. As a result, the survey started on the 25th from the western side of the bay. The winds continued into the 26th and increased to over 30 km/hr while the eastern section of the bay was surveyed.

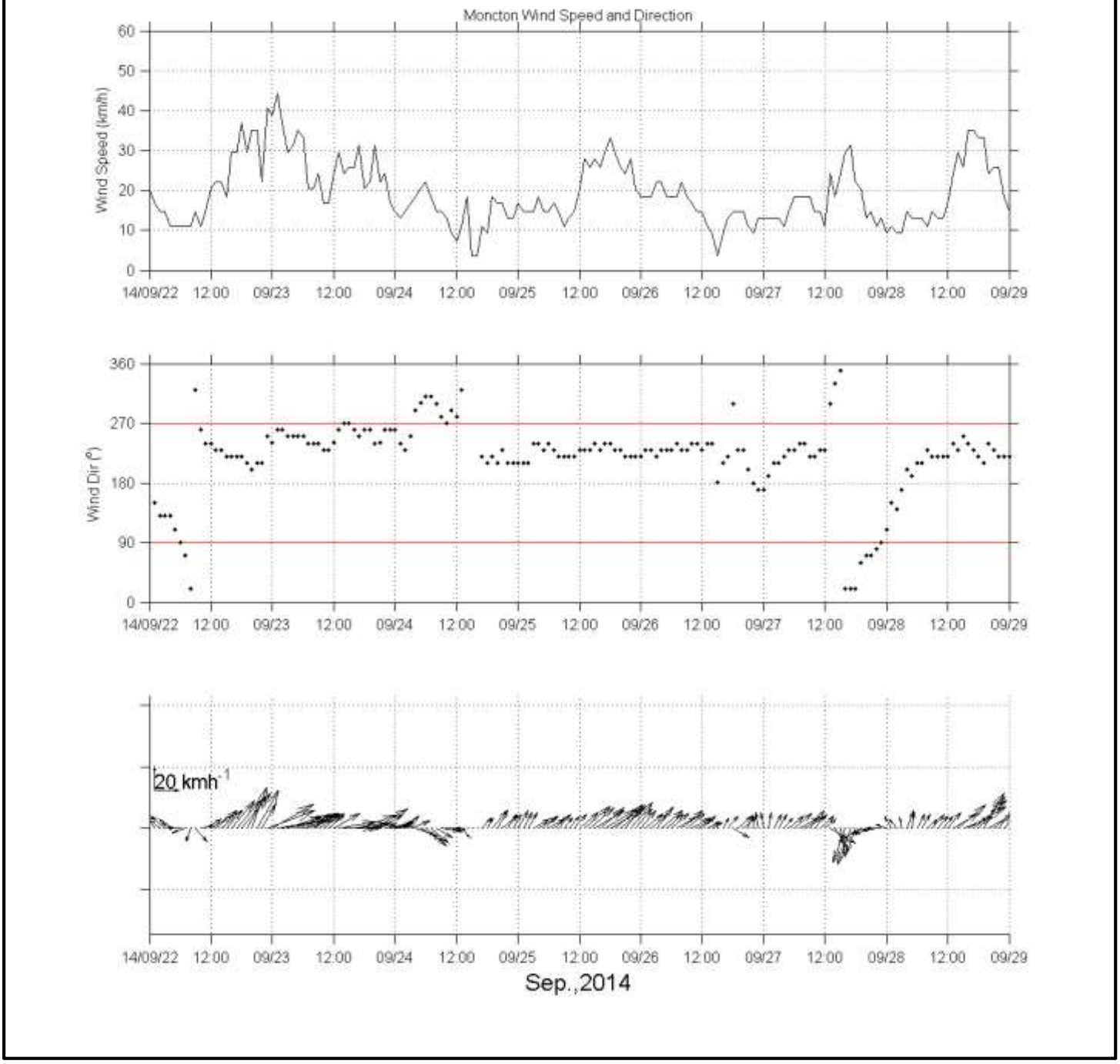

Figure 7: Wind speed (top panel) and direction (middle panel, where the wind is blowing from the direction shown) from Environment Canada weather station at Moncton, NB. The lower panel shows vectors representing the direction the wind is blowing towards. Note the lower wind speeds proceeding and during the lidar flights on Sept. 25 and 26.

2.4 Lidar Data Processing

2.4.1 Lidar point processing

Once the GPS trajectory was processed for the aircraft utilizing the GPS base station and aircraft GPS observations and combined with the inertial measurement unit, the navigation data was linked to the laser returns and georeferenced. Lidar

Survey Studio (LSS) software accompanies the Chiroptera II sensor and is used to process the lidar waveforms into discrete points. The data were processed separately for the two days since they each had a unique trajectory. Each day of collection was inspected to ensure there was sufficient overlap and no gaps exist in the lidar coverage (Figure 8, Figure 9).

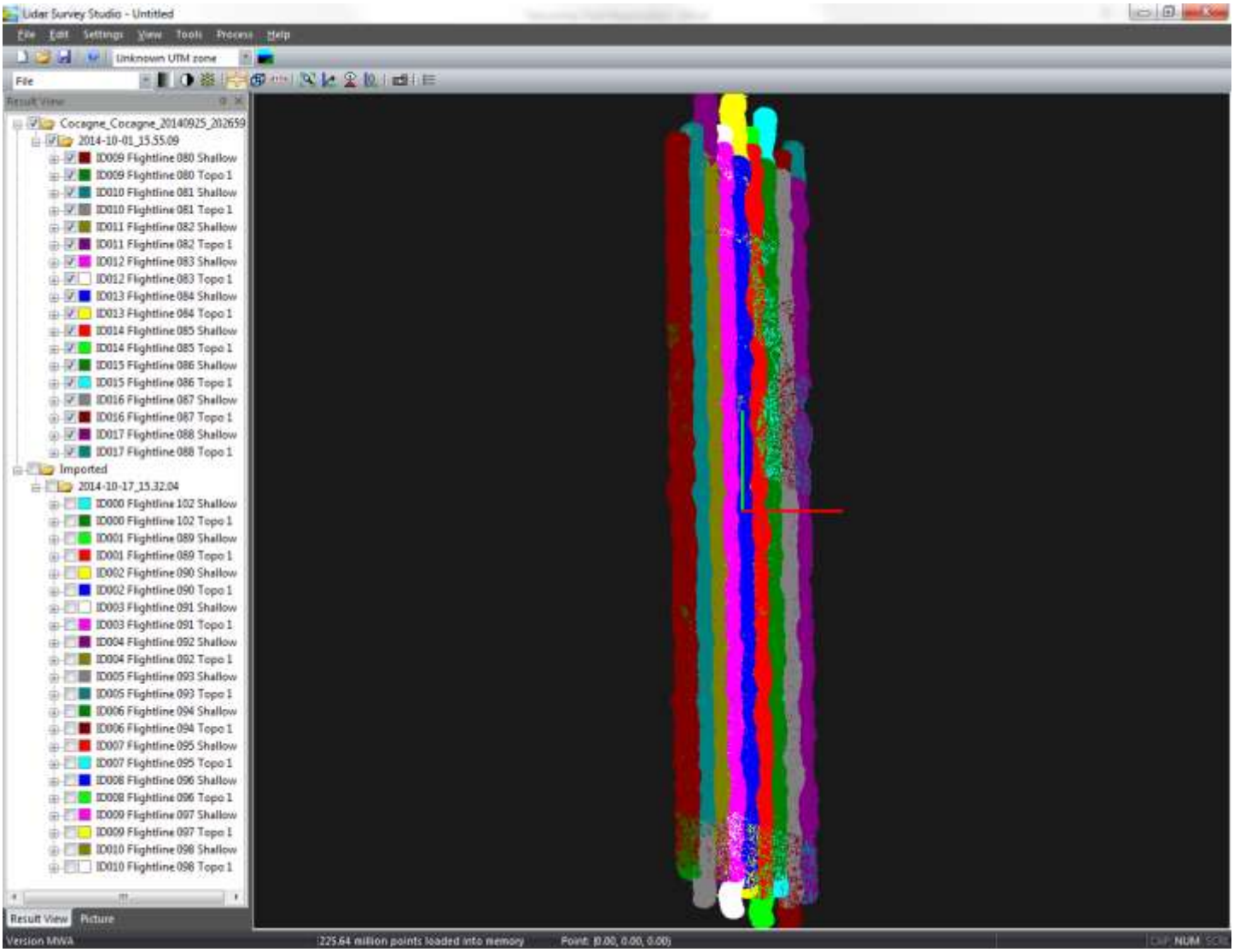

Figure 8 Lidar flight lines day 1, Sept. 25, Cocagne Bay.

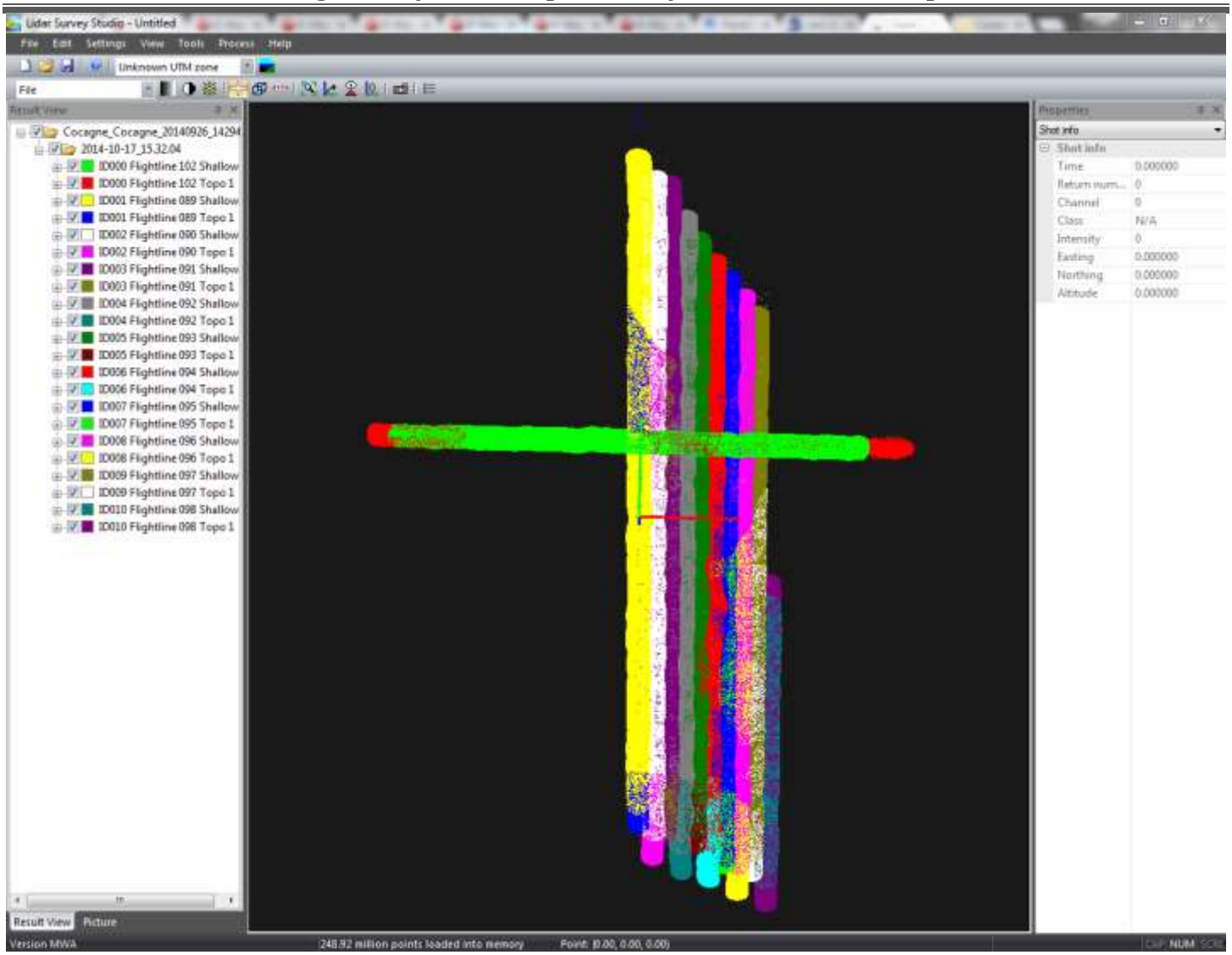

Figure 9 Lidar flight lines day 2 Sept 26, Cocagne Bay.

One critical step in the processing of bathymetric lidar is the ability to map the water surface. This is critical for two components of georeferencing the final target or targets that the reflected laser pulse recorded: the refraction of the light when it passes from the medium of air to water and the change in the speed of light from air to water. The LSS software computes the water surface from the lidar returns of both the topo (TD) and hydro (HD) lasers. In addition to classifying points as land, water surface or bathymetry, the system also computes a water surface that ensures the entire area of water surface is covered regardless of the original lidar point density. As mentioned, part of the processing involves converting the raw waveform lidar return time series into discrete classified points using LSS signal processing; points include ground, water surface, seabed, etc. Once the points were processed in LSS they were imported into Terrascan for further refinement and classification. The following classes have been defined in the final LAS files (Table 2).

Table 2 Tables of classes of the LAS files.

Class number	Description
0	Water model
1	Bathymetry (Bathy)
2	Bathy Vegetation
3	N/A
4	Topo laser (TD) Ground
5	TD non-ground (vegetation & buildings)
6	Hydro laser (HD) Ground
7	HD non-ground
8	Water
9	Noise
10	Overlap Water Model
11	Overlap Bathy
12	Overlap Bathy Veg
13	N/A
14	Overlap TD Ground
15	Overlap TD Veg
16	Overlap HD Ground
17	Overlap HD Veg
18	Overlap Water
19	Overlap Noise

2.4.2 Gridded Surface Models

The classified points are analyzed and further refined and filtered to reduce noise and eventually converted into a raster surface at a 2 m spatial sampling interval using ArcGIS based on a single continuous dataset for each attribute (reflectance and elevation). Examples of the gridded surface models from the hydro laser include the seabed reflectance (Figure 10) and from the hydro and topo laser for the digital elevation model (DEM) (Figure 11). The original elevations are referenced to the NAD83 ellipsoid, the DEM has been converted so that the elevations are orthometric heights and referenced to the Canadian Geodetics Vertical Datum, of 1928 (CGVD28). In addition to the colour shaded relief DEM, we have also constructed a prodyuct for rapid visual interpretation where the lidar reflectance or intensity is merged with the colour shaded relief maps.

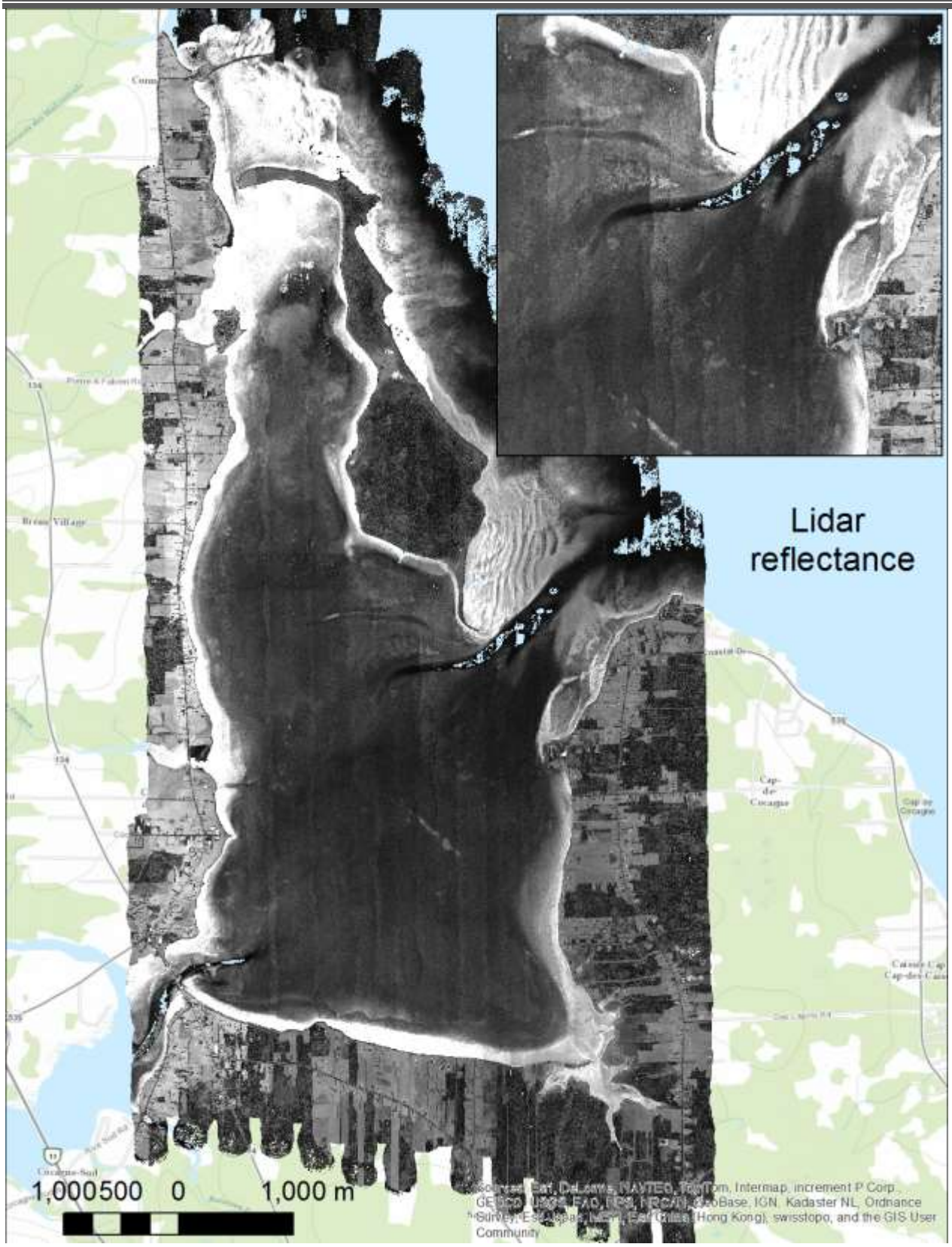

Figure 10 Example of the green lidar seabed reflectance. High values of reflectance indicate more light is being reflected (less light being absorbed, e.g. bright materials like sand), and low values indicate less light is being reflected (more light being absorbed, e.g. dark materials like eelgrass).

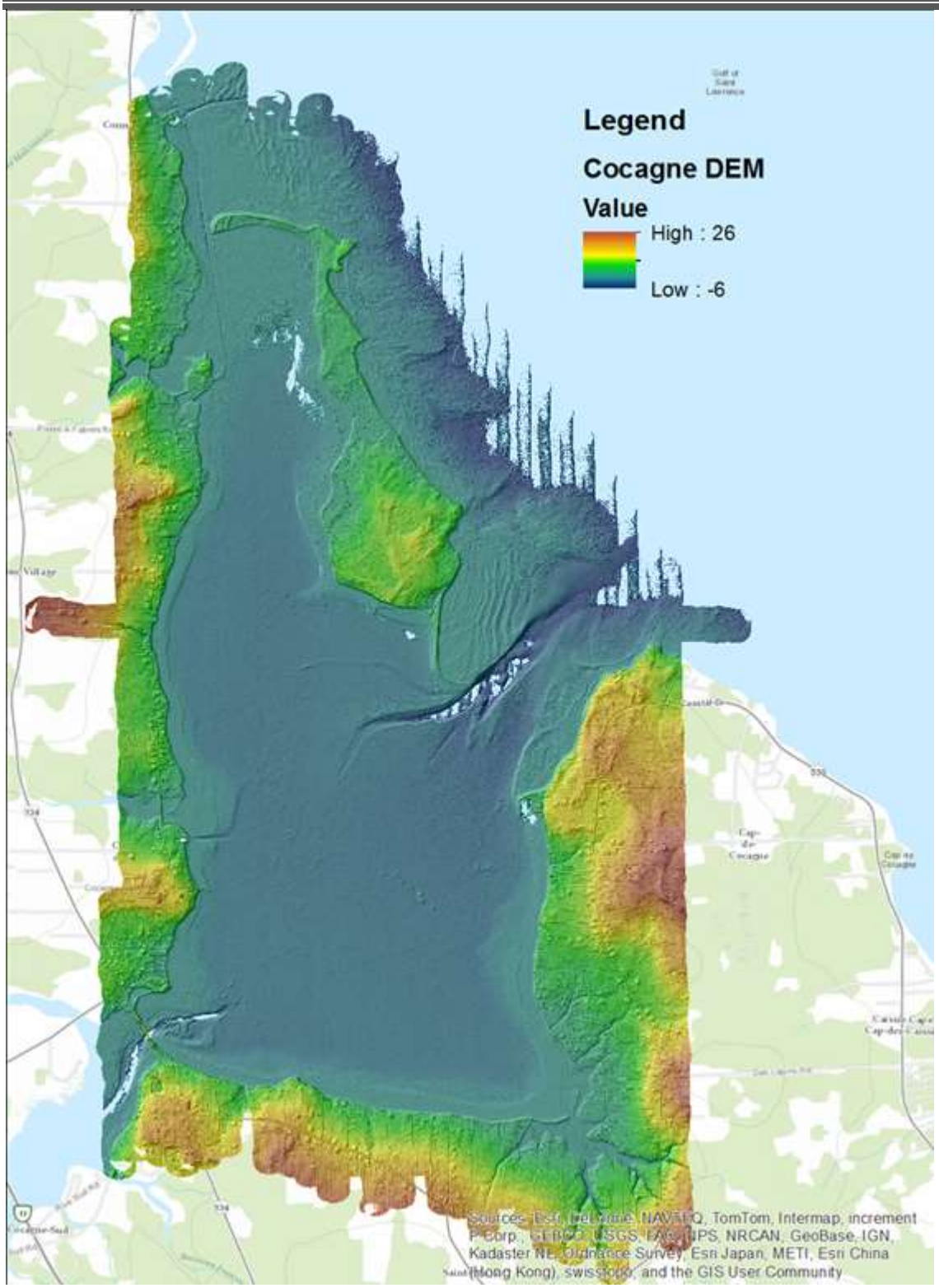

Figure 11 Lidar derived topo-bathymetric map, elevations are orthometric height referenced to CGVD28.

2.4.3 Aerial Photo Processing

The RCD30 60 MPIX imagery was processed using the aircraft trajectory and direct georeferencing. The low altitude and high resolution of the imagery required that the lidar data be processed first to produce a bare-earth digital elevation model (DEM) that was used in the orthorectification process. The aircraft trajectory, which blends the GPS position and

the IMU attitude information into a best estimate of the overall position and orientation of the aircraft during the survey is used to process the air photos. This trajectory, which is linked to the laser shots and photo events by GPS based time tags, is used to define the Exterior Orientation (EO) for each of the RCD30 aerial photos that were acquired. The EO, which has traditionally been calculated by selecting ground control point (x,y, and z) locations relative to the air photo frame and calculating a bundle adjustment, was calculated using direct georeferencing and exploiting the high precision of the navigation system. The EO file defines the camera position (x,y,z) for every exposure as well as the various rotation angles about the x,y and z axis known as omega, phi and kappa. The EO file along with a DEM can be used with the aerial photo to produce a digital orthophoto. Initially processing was attempted to produce the orthophotos without the lidar DEM. This resulted in orthophotos from adjacent frames not lining up. After the lidar data was processed and classified into ground points, the lidar-derived DEM (above and below the water line) was used in the orthorectification process in Erdas Imagine software and satisfactory results were produced. An example from another mission area of the relative alignment between the photos can be seen in Figure 12. In figure 12, the GPS tripod (yellow legs) is setup over our temporary benchmark. The location of the tripod yellow legs and GPS antenna (white dot) move because of the different perspectives of the photo frames and flight lines. A green triangle has been drawn on the figure to represent the base of the tripod and the green dot represents the GPS benchmark on the ground. These features do not change significantly in the photos from frame to frame demonstrating the accuracy of the resultant orthophotos (Figure 12).

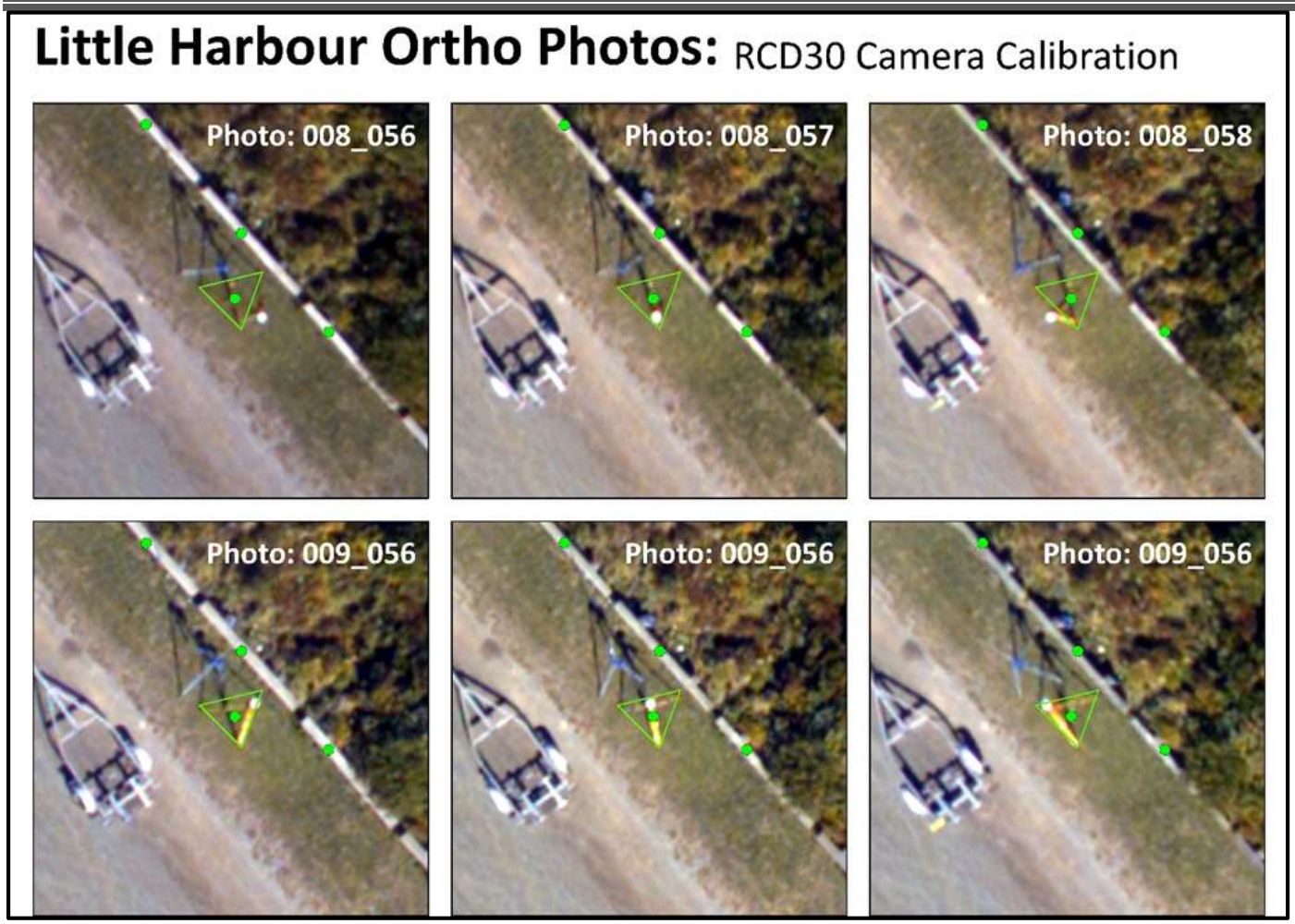

Figure 12 Example of multiple frames (56, 57, and 58) from multiple flight lines (008 on top and 009 below) of the GPS base station location at Little Harbour after orthorectification. The green dots are GPS locations along the parking lot rail and the aircraft control benchmark on the ground below the tripod where the bottom of the legs are represented by the green diamond.

2.4.4 Lidar Validation

Various GPS checkpoints were collected to compare to the lidar points and surface models to ensure the vertical accuracy of the data was sufficient. The GPS elevations were converted from ellipsoidal height to orthometric heights using HT2 within Leica GeoOffice. These GPS points that represent the bare ground were then overlaid with the lidar DEM and the raster cell value appended to the point file. The difference in elevation between the GPS point and the lidar derived DEM was then computed and summary statistics calculated. The delta Z values, or DZ, can then be displayed graphically on the map. The results of the validation will be shown in the results section.

2.5 Digitizing Aquaculture

Aquaculture for the Cocagne Bay area was digitized manually into lines utilizing the five cm resolution orthophoto mosaic with enhancements applied in ArcMap to make subsurface cage identification possible. Measurements that were taken for each different cage type include width, height, and average space between each cage along the line.

2.5.1 Cage Types

After all aquaculture had been digitized several potential different cage types were detected. Photos of each cage, along with dimensions, were sent to Monique Niles of DFO Moncton to be identified. Of the potential cage types many were identified as spat collectors which were not to be included in biomass estimates. Four unique cage types were identified as requiring biomass estimates.

2.5.2 OysterGro Cages

By far the most prominent type of cage identified were OysterGro cages, of 636 total digitized lines 452 were identified as OysterGro cages. The majority of these cages were located on the water surface but a small percentage, 91 of the 429 lines, were subsurface. OysterGro cages measure 1.4m x 0.9m with an average line spacing of five meters; each cage contains six oyster bags. Figure 13 shows the OysterGro cages in it's various positions.

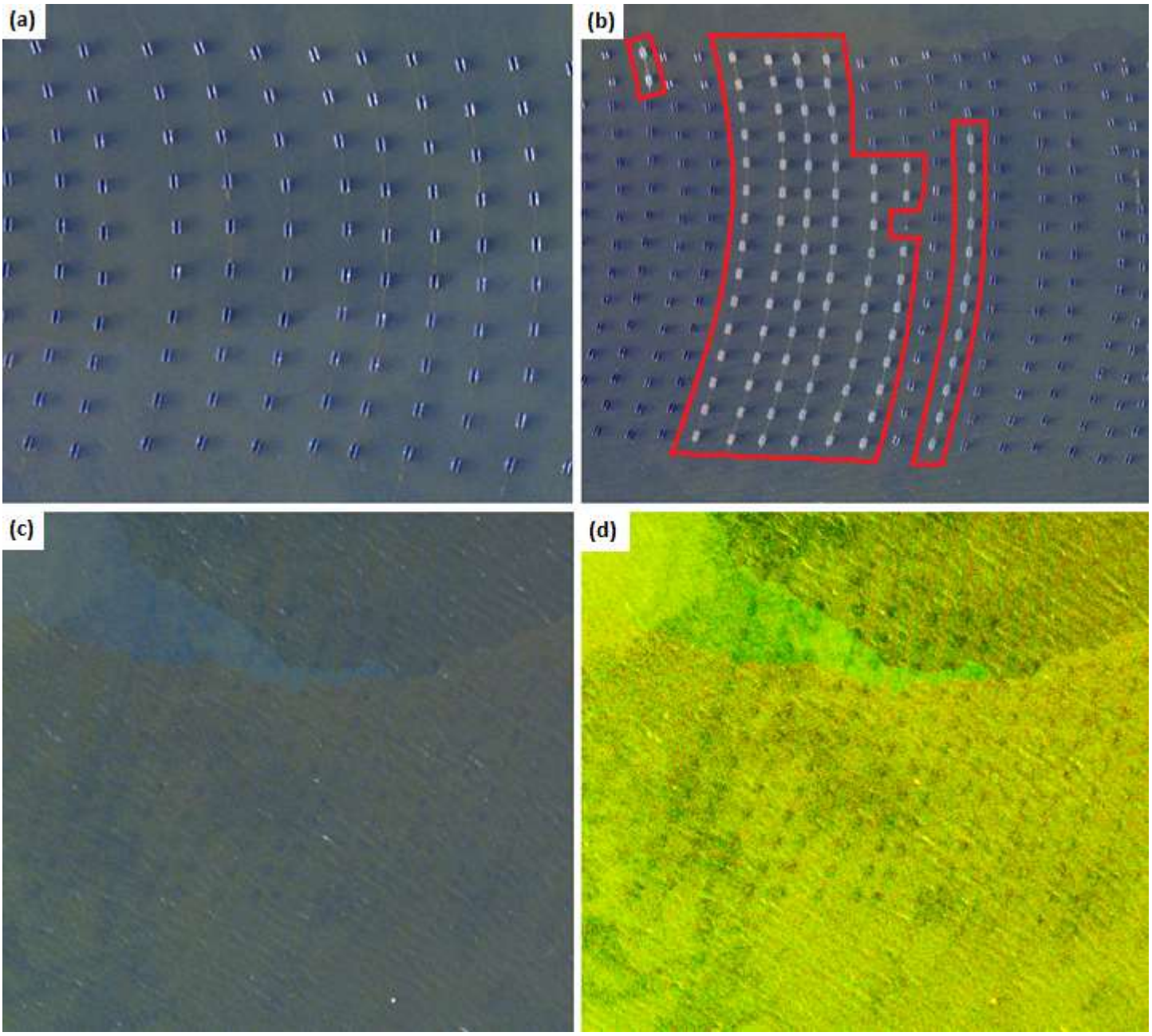

Figure 13 In this figure (a) shows lines of OysterGro cages rightside up, (b) shows some upsidedown cages (outlined), (c) is an image of subsurface cages with no enhancement, and (d) is the same image with the enhancement applied for digitizing purposes.

2.5.3 French Oyster Tables

Located in the northern area of the bay a group of French oyster tables were located. Most cages appear to be just below the surface of the water, a few appear to have the top exposed above water. French oyster tables measure 2.8m x 0.85m with an average line spacing of 3.2m between cages; each cage contains 6 oyster bags. Figure 14 shows several images of French oyster tables.

Figure 14 Several images of French oyster tables in the northern area of Cocagne Bay

2.5.4 Large Rafts

Two types of floating raft style cages were identified in Cocagne Bay. The larger of these contains 12 cages per floating raft; some cages were seen above water and others submerged. Cage dimensions are 0.9m x 1.5m with an average space between of 1m; each cage contains 12 oyster bags. Figure 15 shows several images of large raft cages, some above water, some below.

Figure 15 Large raft cages, some submerged, others above the water surface

2.5.5 Small Rafts

The second type of floating raft that was identified is smaller, holding 6 cages per raft. Again some of the cages are shown to be above water and others subsurface. The cage dimensions differ from the larger raft coming in at 0.6m x 2m with an average spacing of 0.85m; each cage contains 10 oyster bags. Figure 16 shows several images of small raft cages, some above water, some below; the left image shows a comparison of the size difference between the rafts.

Figure 16 The left image shows a comparison in size of the larger raft (leftmost raft) and the smaller raft, the smaller rafts have cages above and below the water (right image).

2.6 Eelgrass Mapping

The eelgrass map for Cocagne Bay was generated using the five cm orthophotos and a one meter depth grid which was derived from Lidar data. A formula which utilizes the depth grid is applied to the red channel of the orthophoto to create the eelgrass presence and absence map. Aerial photograph information was preferentially used in areas of shallow water (sub metre depth) where bathymetric backscatter amplitude (reflectance) exceeded the threshold of the sensor (white wash). Conversely, in areas of deeper water (greater than 1 metre) reflectance information from the bathymetric laser backscatter was preferentially used over aerial photography. To facilitate this, both datasets (aerial photograph and lidar reflectance) were developed with confidence values, a function of depth such that:

$$\frac{\sqrt{depth - a}}{(depth + 1)^{depth/b}}$$

Whereas: *depth* is the water depth at the time of data acquisition (as determined by the bathymetric lidar data, in metres depth); a is an offset factor of data confidence with depth; and, *b* is the peak confidence depth or slope. By applying the above described depth confidence factoring to both the aerial photograph and lidar reflectance models, a singular hybrid radiometric dataset can be generally seamlessly whereas aerial photograph values represent the shallow water areas, and

bathymetric lidar reflectance represents the deeper portions of the study area. Depth confidence curves for each of the two datasets were determined experimentally by observing the distribution of signal/noise ratio and other factors.

Prior to eelgrass analysis, both data (aerial photograph and lidar reflectance amplitude) were individually compensated for water column attenuation using an experimentally derived logarithmic function which is designed to increasingly raise the resultant reflectance values (lidar or aerial photograph) as a function of depth (depth which is determined from bathymetric lidar). This effect allows for the partial removal of the component of the lump radiometric signal from data which represent the signature of the water column on a cell by cell basis. The result is a much more distinguishable bottom image at greater depths.

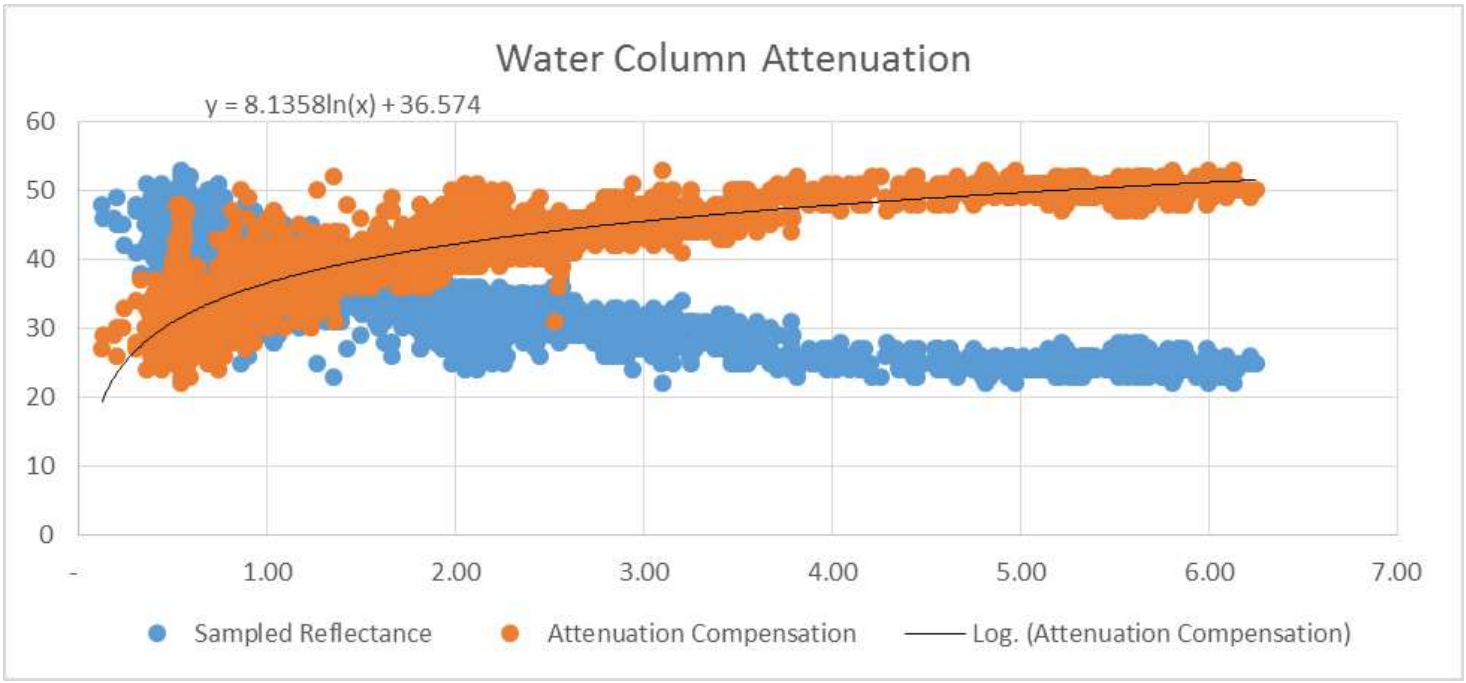

Figure 17 Graph showing the attenuation of the signals due to the water column.

Figure 17 shows an example of a water column attenuation compensation function as derived from sample reflectance points from aerial photograph. Samples are taken along features of an assumed similar true reflectance (sand bottom) and along lines of increasing depth. Depth information is based on the continuous depth map derived from the simultaneously captured bathymetric lidar data.

To facilitate further analysis, the singular raster dataset (which is built from the described hybrid of bathymetric lidar reflectance and aerial photography) classification is performed such that low values are considered more likely submerged vegetation (darker depth normalized underwater features) and high values are considered more likely bright sediment (lighter depth normalized underwater features). Given the seemingly low distribution of sediment reflectance values distributed throughout the (as determined visually from aerial photograph), this simple threshold reflectance method generates good results for underwater vegetation mapping in this area. Further analysis may be required to further differentiate underwater species specifically (ie, eelgrass vs. others.)

3 Results

The GPS trajectory information for the aircraft from each day has been processed and used in processing the lidar and aerial photography. A seamless Digital Elevation Model has been constructed from a combination of the topo and hydro laser data and orthophotos have been processed from the aerial photographs. The lidar reflectance has also been constructed from lidar point data.

3.1 Lidar Point Cloud Features

The lidar point cloud was processed in LSS and then further refined in Terrascan. The LAS files from LSS were used to construct project blocks within Terrascan that facilitated the processing and filtering of the data. The LSS files have elevation referenced to the NAD83 ellipsoid. The LAS points for all the classes with the exception of the noise classes have also been written out as ASCII files consisting of class number (Table 2), x, y, z, intensity, where the x,y are UTM Zone 20 NAD83 and z is height above the NAD83 ellipsoid.

3.2 Lidar Surface Models

The lidar surface models have been constructed from the classified points to represent:

1. A continuous Digital Elevation Model (DEM) from land to the submerged seabed (Figure 18)
2. A continuous Digital Surface Model (includes trees, buildings, wharves etc.) from land to the submerged seabed (Figure 19)
3. Lidar reflectance map of the seabed cover type

The DEM and DSM elevations are referenced to CGVD28 where positive is up and negative is down. In addition to the DEM and DSM, colour shaded relief maps were constructed that included the lidar reflectance (Figure 20).

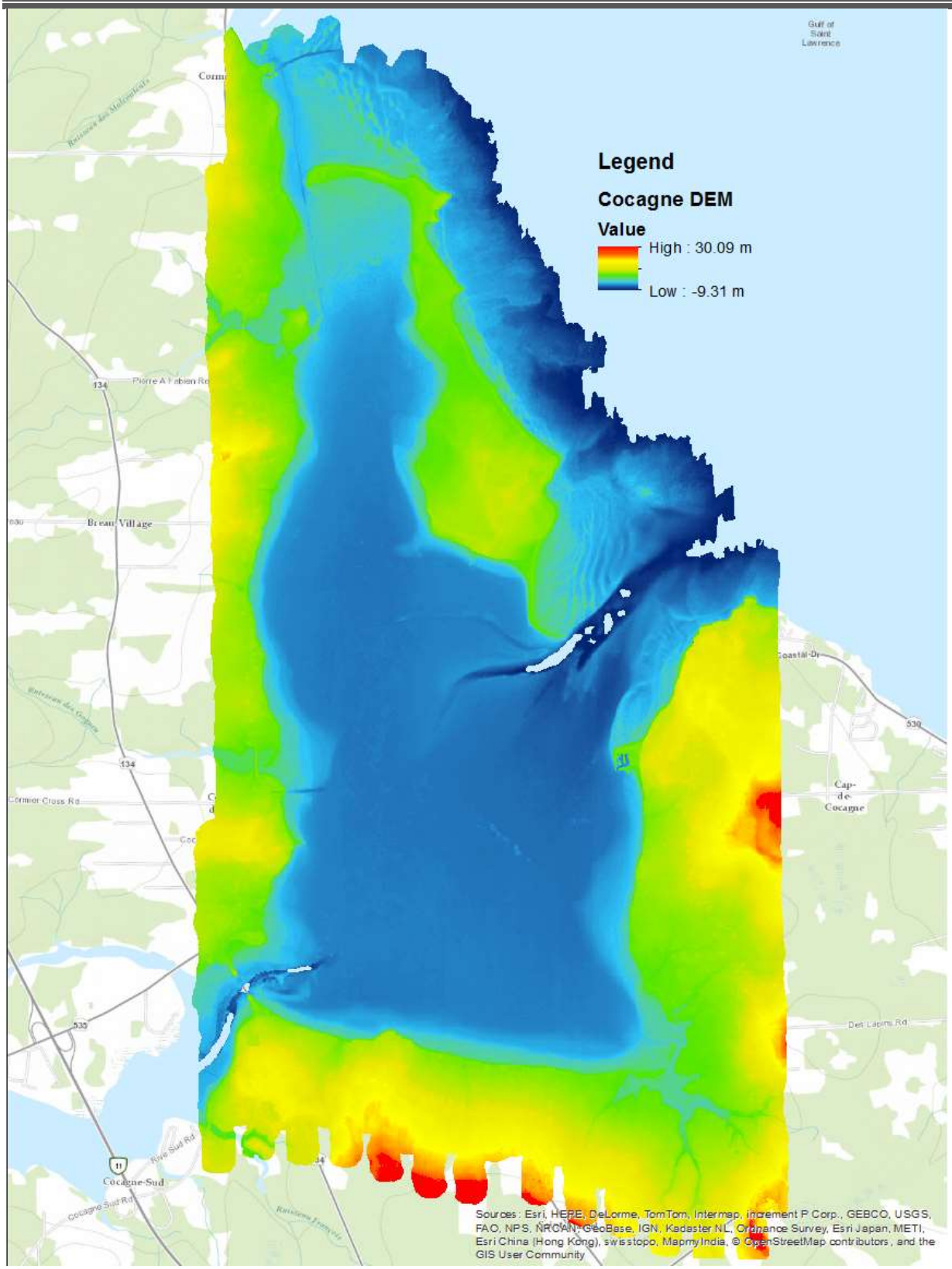

Figure 18 Digitital Elevation Model of Cocagne Bay derived from Lidar data, elevations are orthometric height referenced to CGVD28.

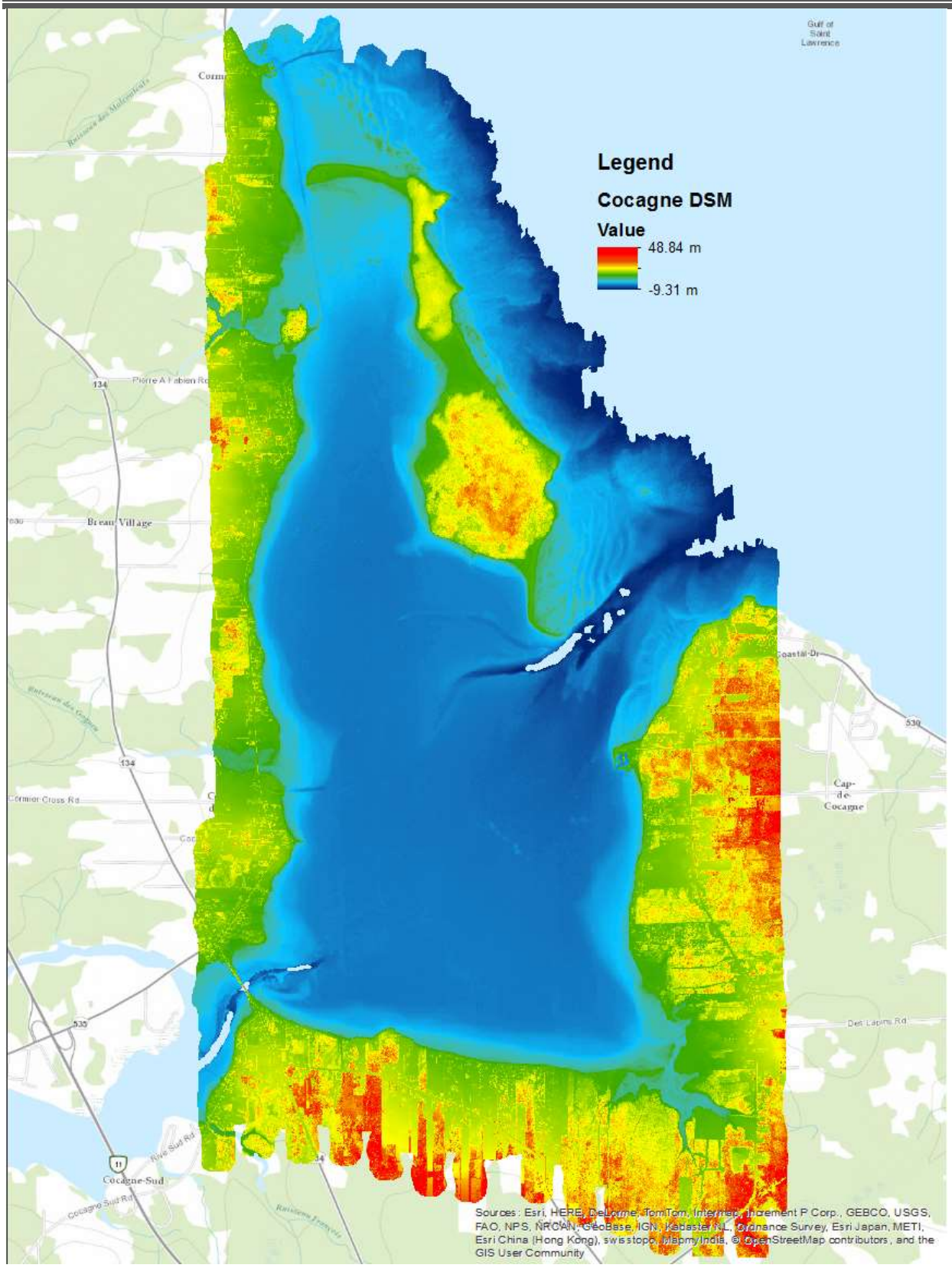

Figure 19 Digital Surface Model of Cocagne Bay derived from Lidar data, elevations are orthometric height referenced to CGVD28.

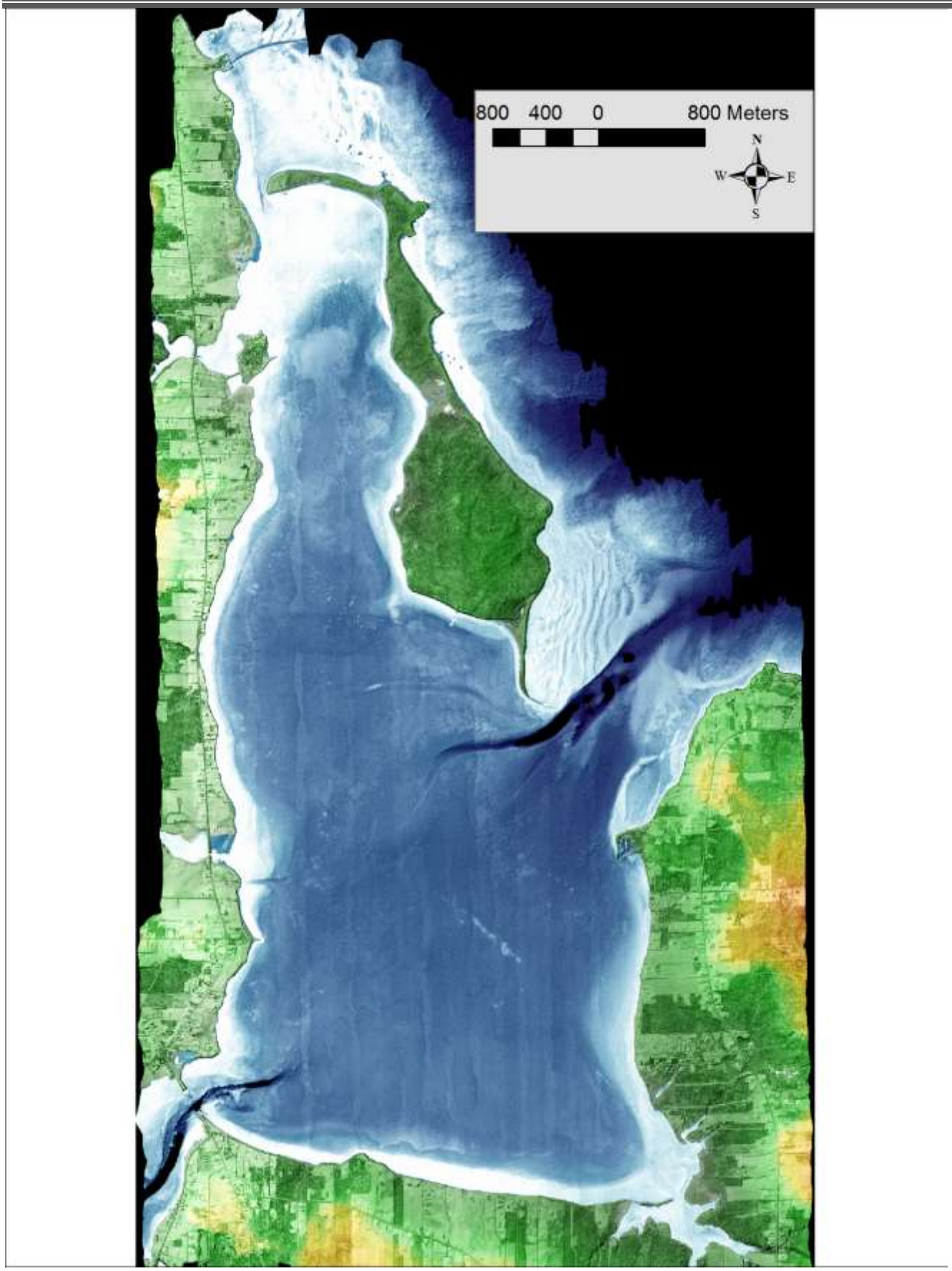

Figure 20 Colour shaded relief DEM with lidar reflectance.

3.3 Orthophoto production

The individual air photo frames from the RCD30 have been processed to orthophoto maps and used to construct a 20 cm mosaic (Figure 21). The mosaic is a GeoTif file consisting of four bands: Red, green, blue, and near infrared. Figure 21 represents a RGB true colour composite of the mosaic.

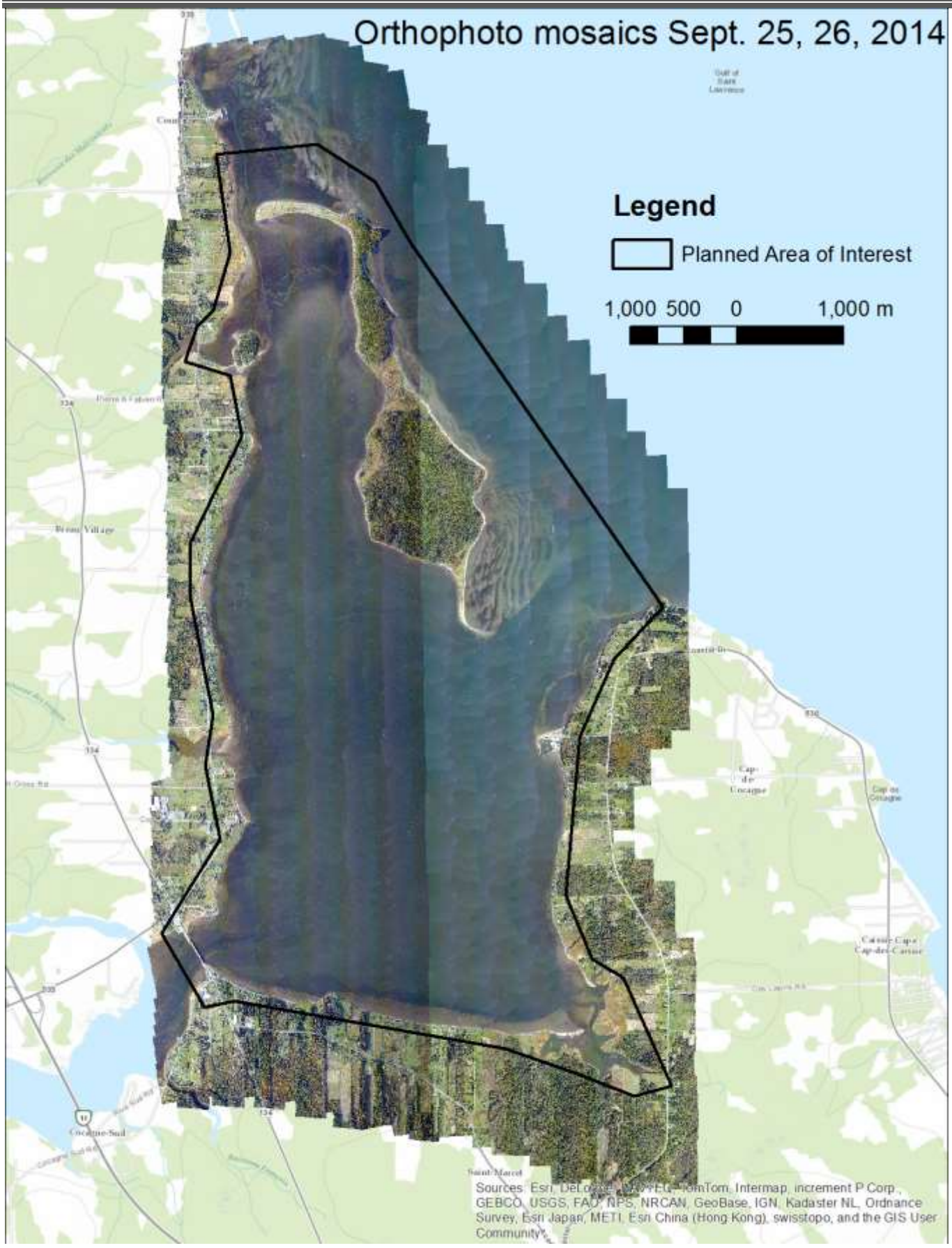

Figure 21 Orthophoto mosaic of Cocagne Bay from Sept 25 and 26.

3.4 GPS Data and Lidar Validation

The GPS checkpoints were overlaid on the lidar DEM and the orthometric height extracted from the DEM to the checkpoint. The difference in elevation between the GPS checkpoint and DEM was computed, DZ = GPS – DEM and colour coded into intervals of differences of 15 cm (Figure 22). A close up of the lidar DEM for the channel is shown in Figure 23. The statistics of the DZ of the checkpoints indicates a mean difference of -0.07 m with a standard deviation of 0.04 m for 7376 points (Figure 24).

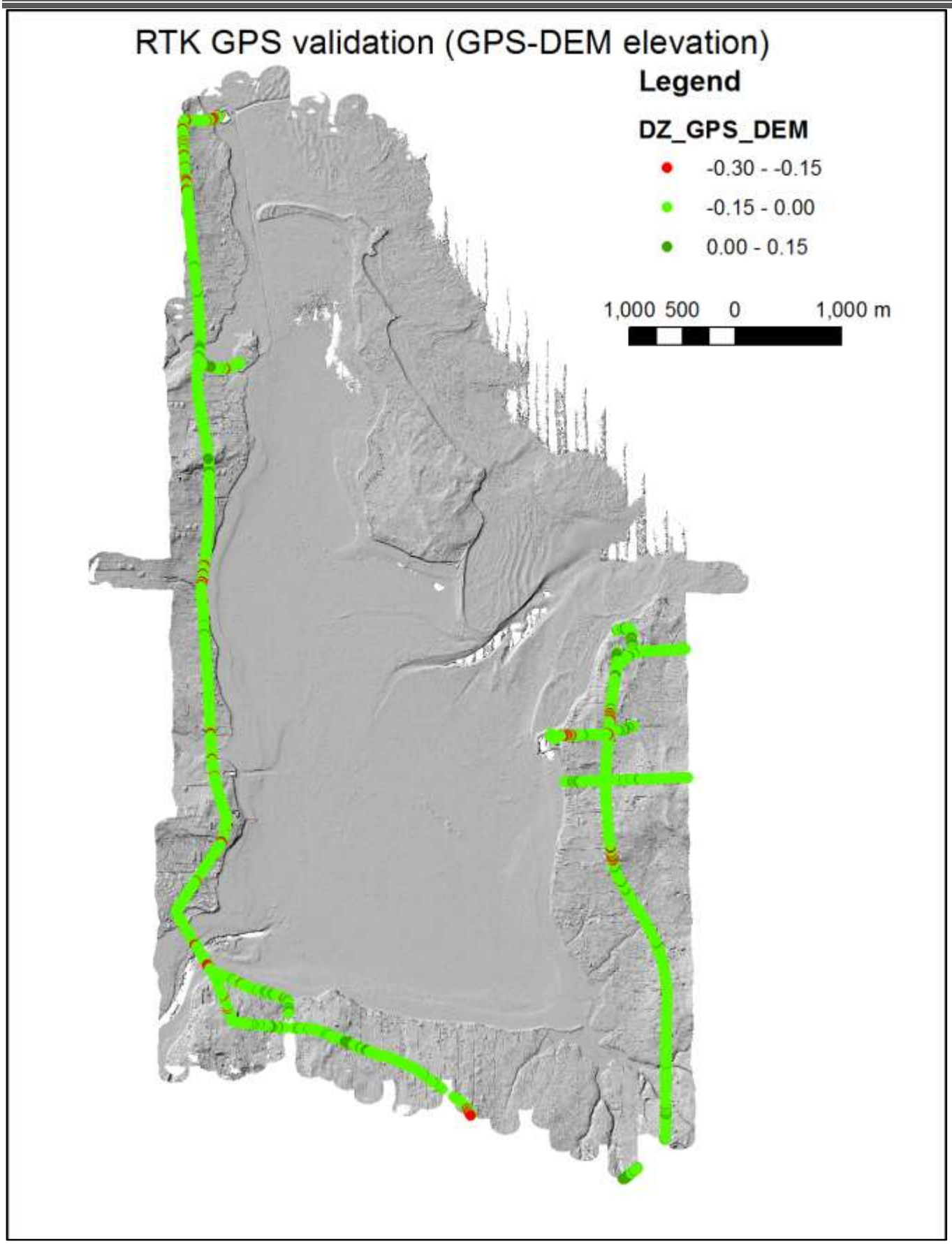

Figure 22 GPS checkpoints colour coded by DZ (GPS-DEM) overlaid on a shaded relief DEM for Cocagne Bay.

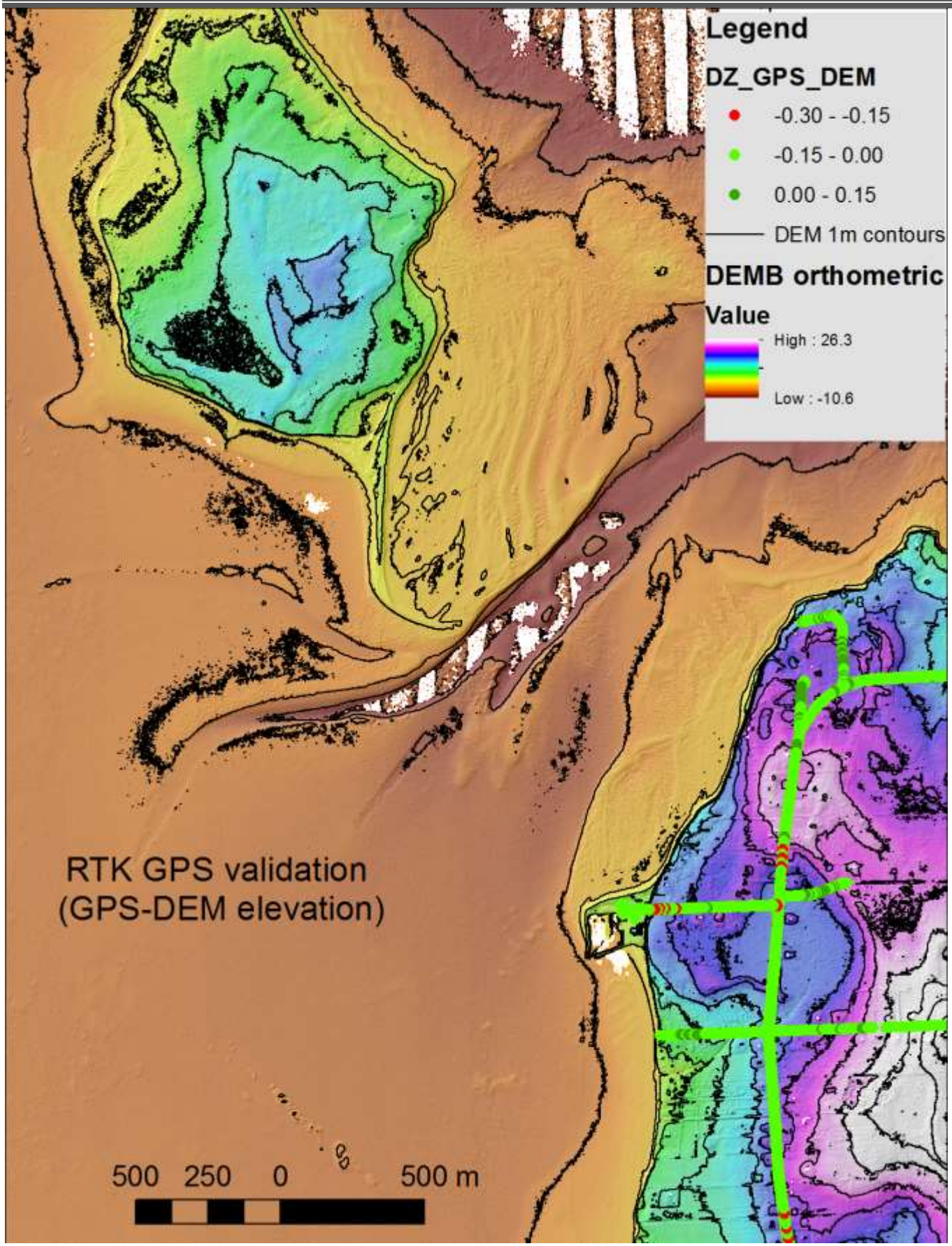

Figure 23 Close up of one meter contours derived from the DEM and GPS checkpoints.

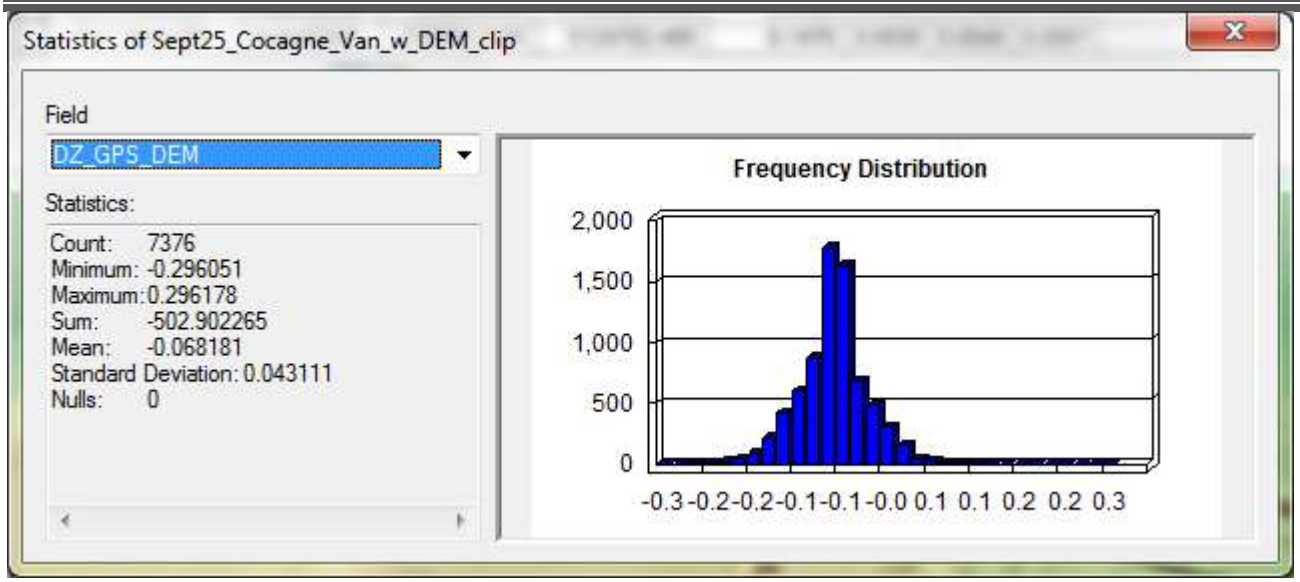

Figure 24 Difference in elevation between checkpoints and lidar DEM (DZ=GPS-DEM).

As can be seen in Figure 24 there is good agreement between the GPS check points and the lidar DEM. Figure 24 shows the frequency distribution of the difference in elevation between the GPS and DEM. The majority of the data show a difference very close to zero and are roughly symmetric about zero. The mean difference in elevation is -7 cm with a standard deviation of four cm for the 7376 checkpoints collected on hard flat surfaces. In general it appears that the DEM may be too high by seven cm, although this difference is well within the specifications of the vertical accuracy of the lidar.

3.5 Depth Intervals

Utilizing the digital elevation model derived from the Lidar point clouds a set of polygons were created for each one meter depth increment below water. Figure 25 shows the contour polygons colorized and displayed over the mosaic. The depth intervals will be used to calculate surface area of the bay in each range as well as eelgrass and aquaculture per meter. The following table shows the total surface area within each depth range:

Table 3 Surface area by depth below watersurface in one meter increments

Depth Below Watersurface(m)	Area(m^2)	Area(ha)
0	6324914.74	632.49
1	3954830.3	395.48
2	11653202.85	1165.32
3	3682617.4	368.26
4	2346798.81	234.68
5	894639.05	89.46
6	9537.69	0.95
7	693.94	0.07
8	349.57	0.03
9	259.95	0.03
10	208.62	0.02
11	160	0.02
12	108	0.01
13	126.63	0.01
14	124	0.01
15	98.02	0.01
16	56	0.01
17	8	0
18	4	0

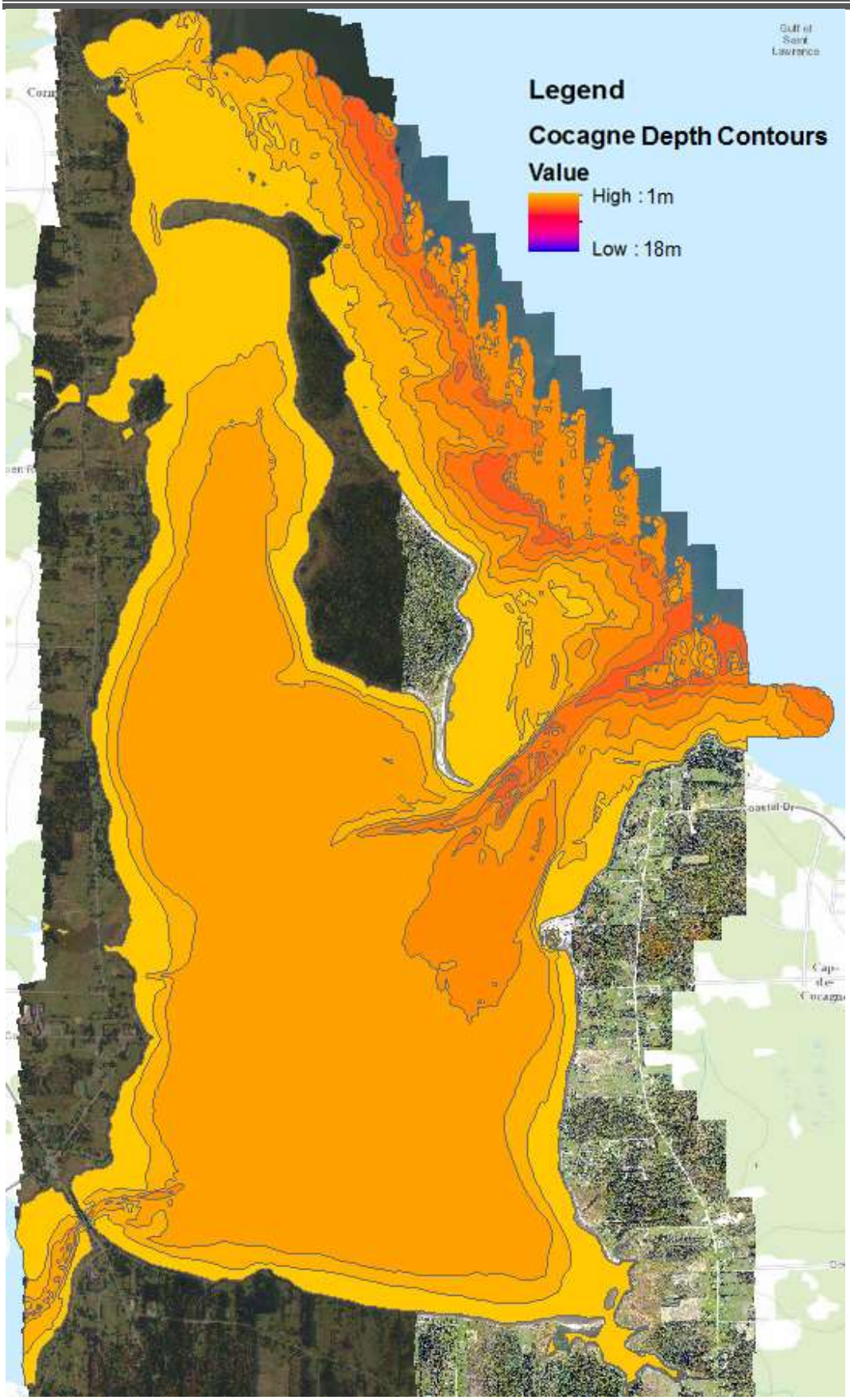

Figure 25 The contour polygons representing depth below water in one meter increments

3.6 Aquaculture Biomass Estimates

Aquaculture biomass estimates were summarized in two different ways: an estimate of total biomass for each cage type, and an estimate for biomass in one meter depth ranges.

3.6.1 Total Biomass Estimate

To create the overall biomass estimate a formula was applied to the digitized aquaculture lines, Figure 26 shows all aquaculture lines digitized within Cocagne Bay. The formula for creating a biomass estimate starts by calculating the number of cages per line by dividing line length by average cage spacing, plus one to compensate for the first cage in the line. The result is multiplied first by the number of bags contained in each cage and then by the 6.04kg biomass estimate per bag given by Monique Niles of DFO Moncton. The formula is expressed as follows:

$$Bio_{Total} = Length / (Spacing + 1) * Bags * 6.04$$

Where: Bio_{Total} = Total Biomass, Length = Length of a given line, Spacing = Space between cages, Bags = Number of bags for the given cage type

The following table shows the results generated by the formula above applied to all digitized aquaculture grouped by different aquaculture:

Table 4 Total cage and biomass estimates

Cage Type	Number of Cages	Biomass Estimate(kg)
OysterGro Cages	3538	128217.12
French Oyster Tables	739	26781.36
Large Rafts	125	9060
Small Rafts	45	2718
Subsurface OysterGro Cages	880	31891.2
TOTAL	**5327**	**198667.68**

Figure 26 Overview of all digitized aquaculture in Cocagne Bay

3.6.2 Biomass Estimate by Depth

Estimates for biomass at one meter depth intervals required dividing the total aquaculture into different shapefiles based on countour polygons created from a modified DEM. Figure 27 shows these lines coloured to indicate the depth range in which the cage resides. The following table shows the resulting aquaculture biomass estimates divided by one meter depth intervals and subdivided by cage type:

Table 5 Cage and biomass estimates by depth

Depth(m)	Cage Type	Number of Cages	Biomass Estimate(kg)
0 to 1	French Oyster Tables	739	26781.36
	TOTAL	**739**	**26781.36**
1 to 2	OysterGro Cages	375	13590
	Large Raft Cages	125	9060
	Small Raft Cages	30	1812
	Subsurface OysterGro Cages	101	3660.24
	TOTAL	**631**	**28122.24**
2 to 3	OysterGro Cages	3168	114808.32
	Small Raft Cages	15	906
	Subsurface OysterGro Cages	781	28303.44
	TOTAL	**3964**	**144017.76**

Figure 27 Digitized aquaculture lines in Cocagne Bay coloured to indicate depth range

When the lines are split along the contour polygon boundaries to create the new shapefiles for aquaculture in each depth range a certain amount of error is introduced as the original line is modified. However, the difference between the total biomass estimate for all cages and the sum of the biomass estimates by range for all cages is quite small, a difference of 254 kg, or 0.13%.

3.7 Eelgrass Mapping

The production of an eelgrass map was complicated because the data were collected over two days and the aerial photography had different sun angles. The depth normalization of the lidar was also complicated as the water represented both inner bay and exposed coastal conditions. However, these complications were overcome to the best of our ability under the timeframe available to conduct the research. An eelgrass map was produced that represents eelgrass within the bay and probably other types of submerged aquatic vegetation along the coast (Figure 28). We interpret this because the substrate along the coast consists of a rocky hard bottom in many locations that is not suitable habitat for eelgrass but maybe fucus.

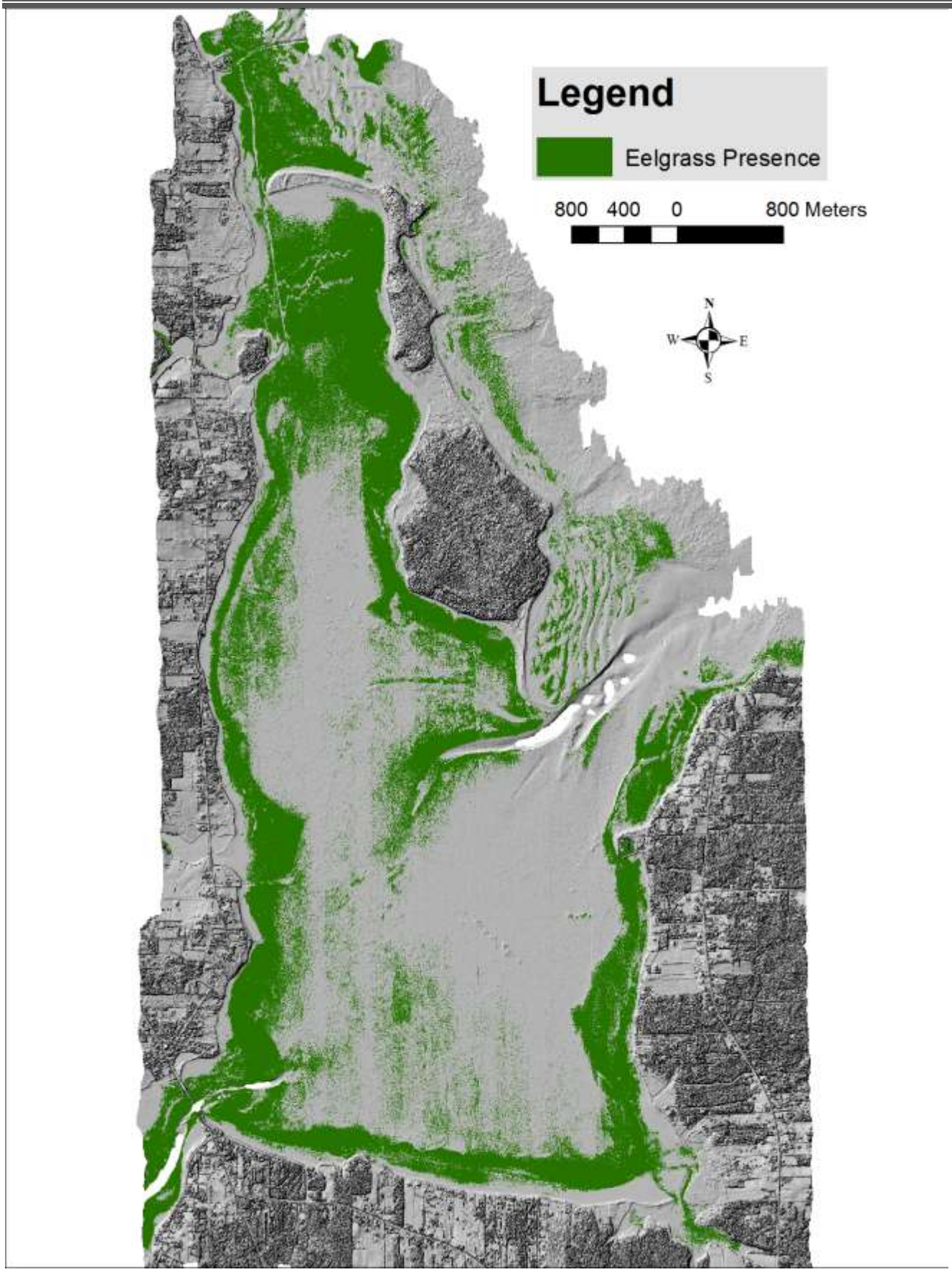

Figure 28 Eelgrass presence map derived from a combination of lidar reflectance and aerial photography. Background is the shaded relief DSM.

The total area of eelgrass within the bay and coastal zone is shown in Table 6.

Table 6 Area of Eelgrass within the study area

Total area (m^2)	Total Area (ha)
7895353.54	789.54

The eelgrass map was overlaid with the depth contour intervals and the area of eelgrass for each contour interval was calculated. The results are shown in Table 7.

Table 7 Area of eelgrass per depth countour interval.

Depth Below Watersurface (m)	Total Area (m^2)	Total Area (ha)
1	3093705.88	309.37
2	2558243.13	255.82
3	2176374.57	217.64
4	331.46	0.03
5	38.92	~0.00
6	6.68	~0.00

The ratio of eelgrass covered area to the total area of each depth contour interval was also calculated and presented in Table 8.

Table 8 Ratio of eelgrass to surface area of each depth contour.

Depth Below Watersurface (m)	Total Eelgrass Area (m^2)	Total Area (m^2)	Ratio
1	3093705.88	6324914.74	1 : 2.04
2	2558243.13	3954830.3	1 : 1.55
3	2176374.57	11653202.85	1 : 5.35
4	331.46	3682617.4	1 : 11110.29
5	38.92	2346798.81	1 : 60298.02
6	6.68	894639.05	1 : 133928

4 Discussion & Conclusions

The researchers at AGRG consider this first mission of the Chiroptera II a huge success and are impressed with the quality of the data sets produced. The lidar data meet the accuracy specifications outlined by the manufacturer and the derived products are of a high quality. Although the orthophotos were taken on separate days in the morning and afternoon the illumination differences between them is not significant. A high level of detail for the aquaculture infrastructure is visible on the orthophotos and were used to quantify the amount of biomass present. The calibration of the lidar sensor is discussed in

Appendix 1 Calibration Report of the Topo-Bathymetric lidar.

In the northern area of Cocagne Bay there are quite a few lines of French oyster tables. Next to several of these lines there is a clearly visible absence of subsurface vegetation. The absence of eelgrass also appears to be approximately the same length, spacing, and shape as the lines of French oyster tables located just next to them. This eelgrass absence is seen most cleary amongst these French oyster tables, however other areas of heavy aquaculture seem to have a lack of eelgrass in close proximity. Figure 29 shows a map of the French oyster tables and outlined areas where eelgrass appears to have been diminished in a pattern similar to that of the accompanying aquaculture.

The current process for mapping eelgrass utilizes the orthophotos and a depth grid derived from Lidar data. This system could use improvement in certain areas where misclassifications are made due to obstructions in the orthophoto such as aquaculture cages, shadows, and unusally dark surfaces. Data stored in the returned waveform profile may be key in increasing accuracy of eelgrass maps. Numerous studies involving the classification of seabed cover types using Lidar data have leveraged the waveform data with marked success. In the future utilizing products derived from return waveform characteristics could provide superior eelgrass maps. For instance the waveform data allows for the recreation of the waveform curve. When the laser from the Lidar hits a surface the angle at which it contacts the surface can determine the peak return reflectance value. If the laser were to strike the surface at a perfectly perpendicular angle then a high peak value would be seen, if the angle were more oblique then the return value would not be as high and the waveform curve would be more spread out. In the case that two different lasers hit the same spot but at different angles the shapes of the waveform curve would be different as would the peak return values but the area under the curve would be the same for both. This means that area under the curve of the waveform may prove to be more representative of the return than the peak return values that are available currently.

In addition to the standard GIS deliverable layers, DEM, orthophotos, lidar reflectance, and these data were used to construct an eelgrass map. As well the high resolution orthophoto mosaic, 5 cm resolution, was used to measure the aquaculture infrastructure and from that estimate the amount of filter feeder biomass for the bay. In addition, the lidar DEM was used to calculate the area of 1 m depth intervals. The eelgrass was then overlaid with the depth intervals and various metrics measured including the ratio of eelgrass to depth area.

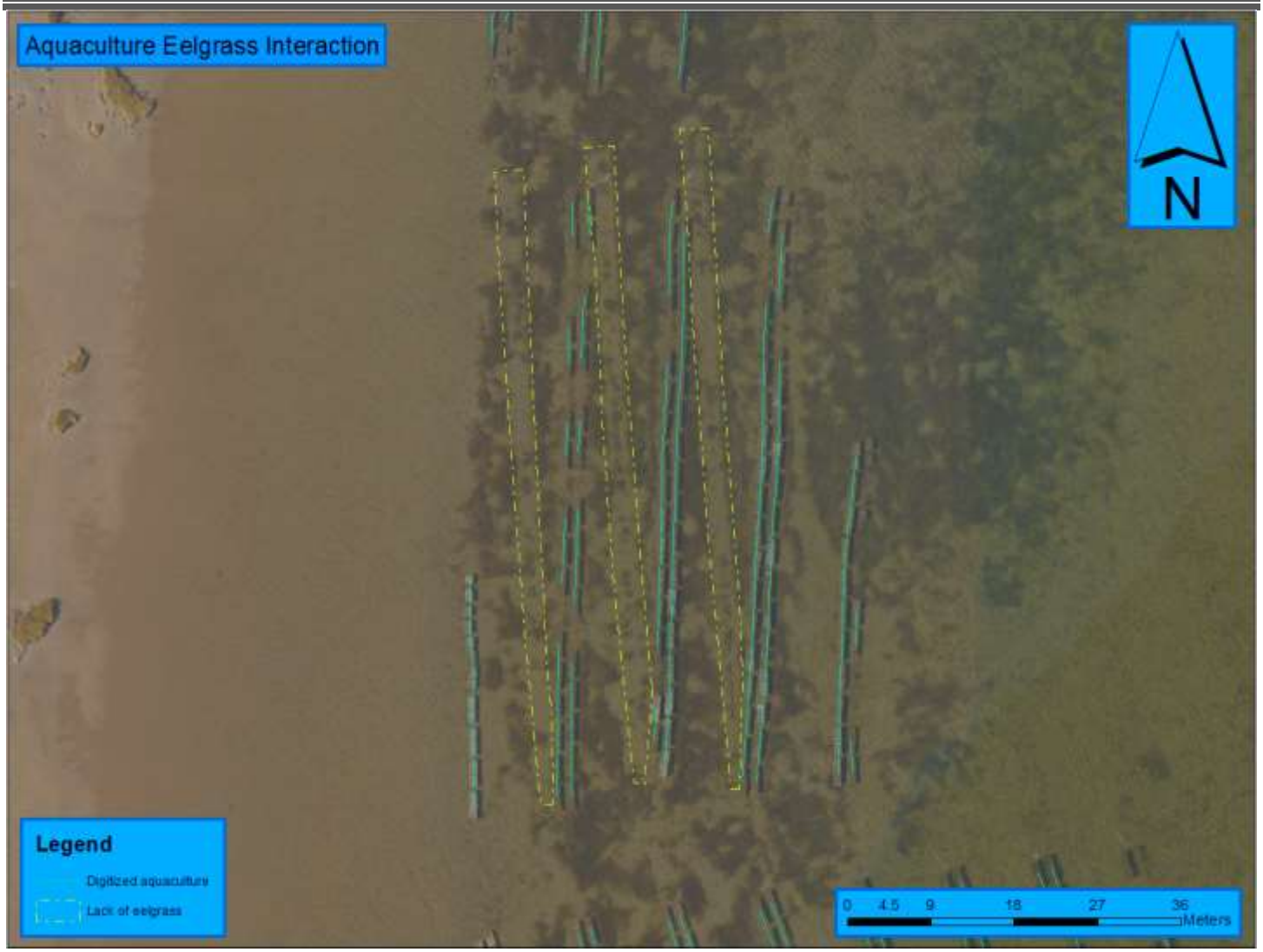

Figure 29 Possible effects of aquaculture on eelgrass in northern Cocagne Bay.

5 References

Carr, J., D'Odorico, P., McGlathery, K. and Wiberg, P. 2010. Stability and bistability of seagrass ecosystems in shallow coastal lagoons: Role of feedbacks with sediment resuspension and light attenuation. JOURNAL OF GEOPHYSICAL RESEARCH, VOL. 115 G03011, doi:10.1029/2009JG001103, 1-14.

Valle, M., Borja, A, Chust, G., Galparsoro, I., Garmendia, J.M. 2011. Modelling suitable estuarine habitats for Zostera noltii, using Ecological NicheFactor Analysis and Bathymetric LiDAR. Estuarine, Coastal and Shelf Science, 94, 144.-154.

6 Appendix 1 Calibration Report of the Topo-Bathymetric lidar

6.1 NSCC – Chiroptera Calibration Report

6.1.1 Calibration flight pattern

Calibration flight was done over the Fredericton downtown area. The calibration pattern consists of 4 lines, 3 parallel and one perpendicular. The middle and perpendicular lines are flown in both directions. The pattern is flown at two altitudes resulting in a total of 12 lines.

GPS base station was taken from the CanNet active network, well within 30 km of the calibration flight plan.

The calibration pattern was flown once at the start of the project and once at the end.

6.1.2 Calibration

Calibration is done in the automatic calibration tool which is part of Lidar Survey Studio.

Reference points were provided by Leading Edge Geomatics.

6.1.3 Results

6.1.3.1 Topo accuracy analysis

Accuracy analysis performed in Lidar Survey Studio using the following settings:

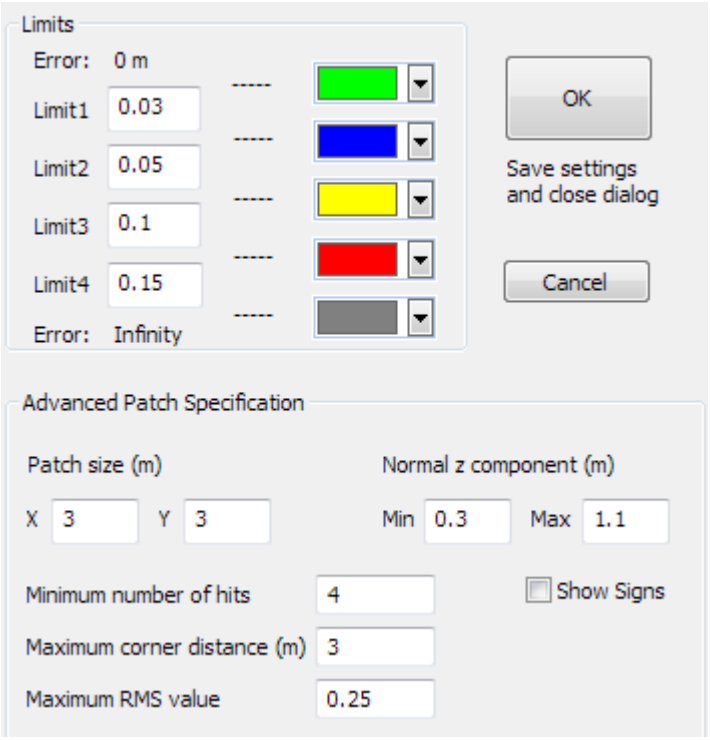

Topo - 400 m

Flightline accuracy between flightline 4 and flightline 2:

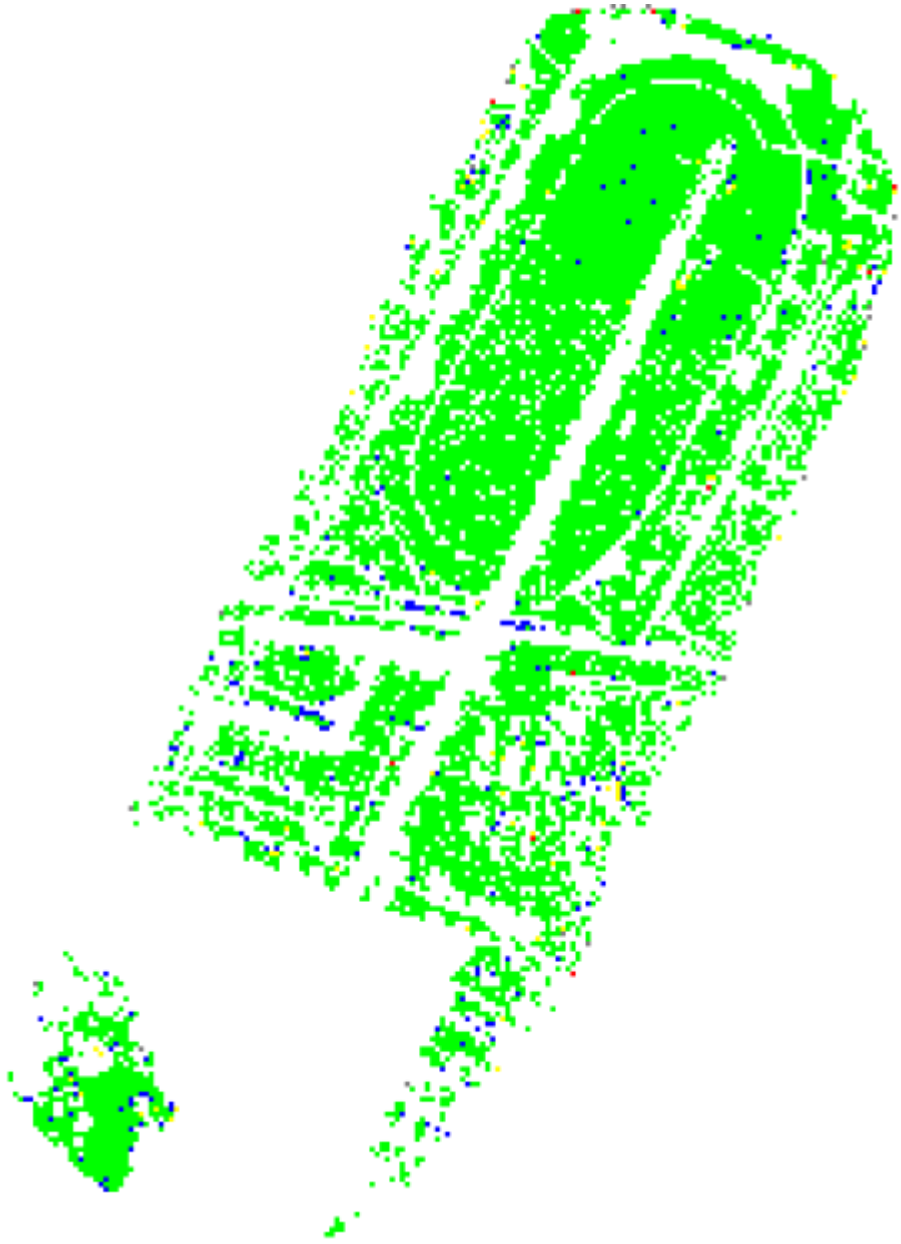

Flightline Accuracy Report Output:
ID003 Flightline 004 Topo 1 vs. ID008 Flightline 002 Topo 1 FL Accuracy

Limits	Patch#	First FL Positive	Average Error	Percentage
0.00 <= ERR <0.03	9748	48.16%	0.0063	96.63%
0.03 <= ERR <0.05	230	46.96%	0.0371	2.28%
0.05 <= ERR <0.10	78	56.41%	0.0657	0.77%
0.10 <= ERR <0.15	10	50.00%	0.1236	0.10%
0.15 <= ERR < Inf.	22	72.73%	0.4768	0.22%
Summary	10088	48.26%	0.0086	

Accuracy Index: 99

Patch Statistics
All#: 44707 | Valid: 26.60% | NumHit.fail:47.15% | ConDist.fail:0.37% | Normalz.fail:18.79% | RMS.fail:7.10%

Flightline accuracy between flightline 5 and flightline 7:

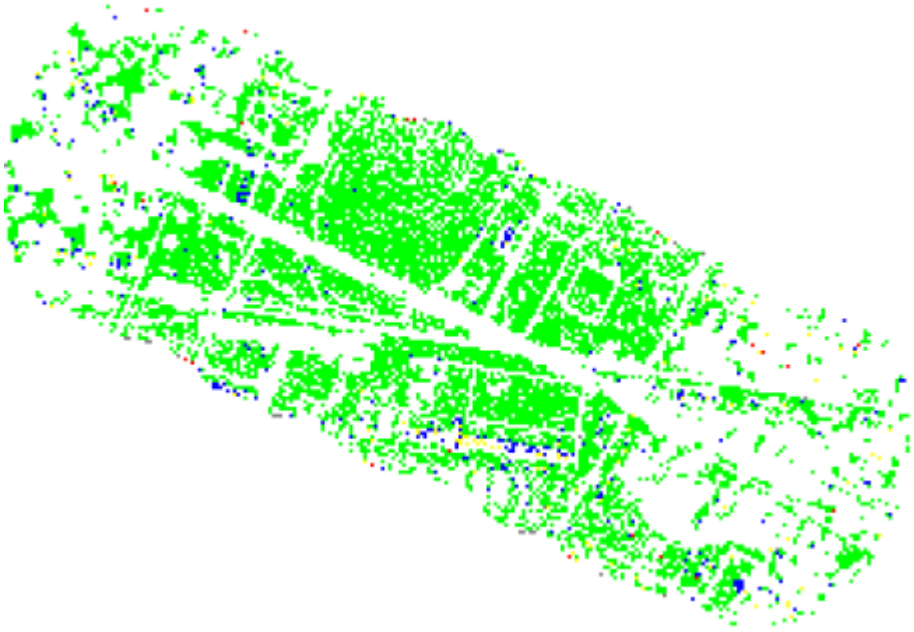

Flightline Accuracy Report Output:
ID005 Flightline 005 Topo 1 vs. ID007 Flightline 006 Topo 1 FL Accuracy

Limits	Patch#	First FL Positive	Average Error	Percentage
0.00 <= ERR <0.03	8505	20.53%	0.0086	94.76%
0.03 <= ERR <0.05	302	18.87%	0.0370	3.36%
0.05 <= ERR <0.10	121	13.22%	0.0640	1.35%
0.10 <= ERR <0.15	21	38.10%	0.1237	0.23%
0.15 <= ERR < Inf.	26	38.46%	0.6219	0.29%
Summery	8975	20.47%	0.0124	

Accuracy Index: 98

Patch Statistics
All#: 46182 | Valid: 23.14% | Nummit.fail:44.79% | Condist.fail:0.26% | Normalz.fail:19.51% | RMS.fail:12.30%

Scan accuracy flightline 4:

Scan Accuracy Report Output:
ID003 Flightline 004 Topo 1+ID003 Flightline 004 Topo 1 Scan Accuracy

Limits	Patch#	Front Scan Positive	Average Error	Percentage
0.00 <= ERR <0.03	10191	65.59%	0.0057	96.85%
0.03 <= ERR <0.05	202	53.47%	0.0381	1.92%
0.05 <= ERR <0.10	79	49.37%	0.0633	0.75%
0.10 <= ERR <0.15	20	65.00%	0.1166	0.19%
0.15 <= ERR < Inf.	31	54.84%	0.3671	0.29%
Summery	10523	65.20%	0.0081	

Accuracy Index: 98

Patch Statistics
All#: 56842 | Valid: 21.69% | NumHit.fail:55.93% | ConDist.fail:0.29% | Normalz.fail:15.57% | RMS.fail:6.52%

6.1.3.2 Hydro accuracy analysis

Accuracy analysis performed in Lidar Survey Studio using the following settings:

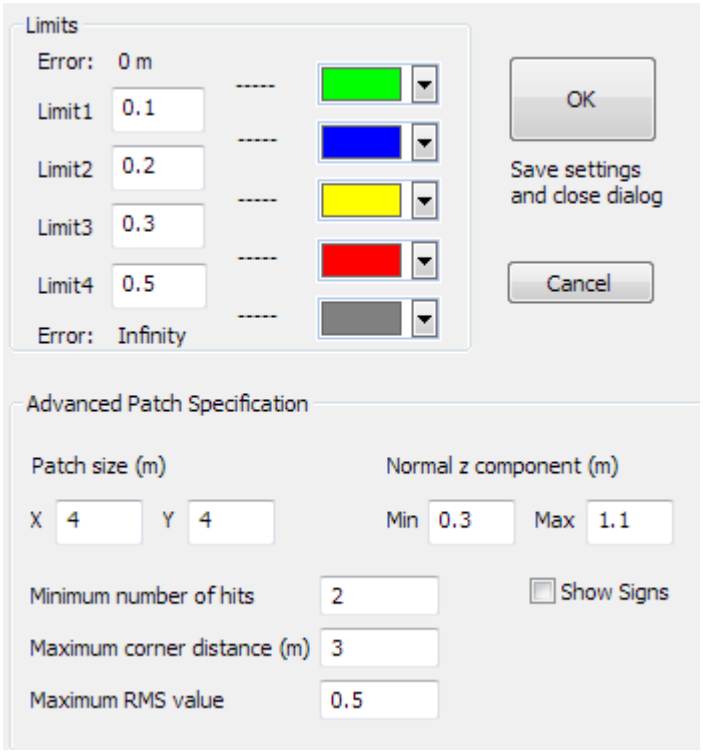

Flightline accuracy between flightline 4 and flightline 2:

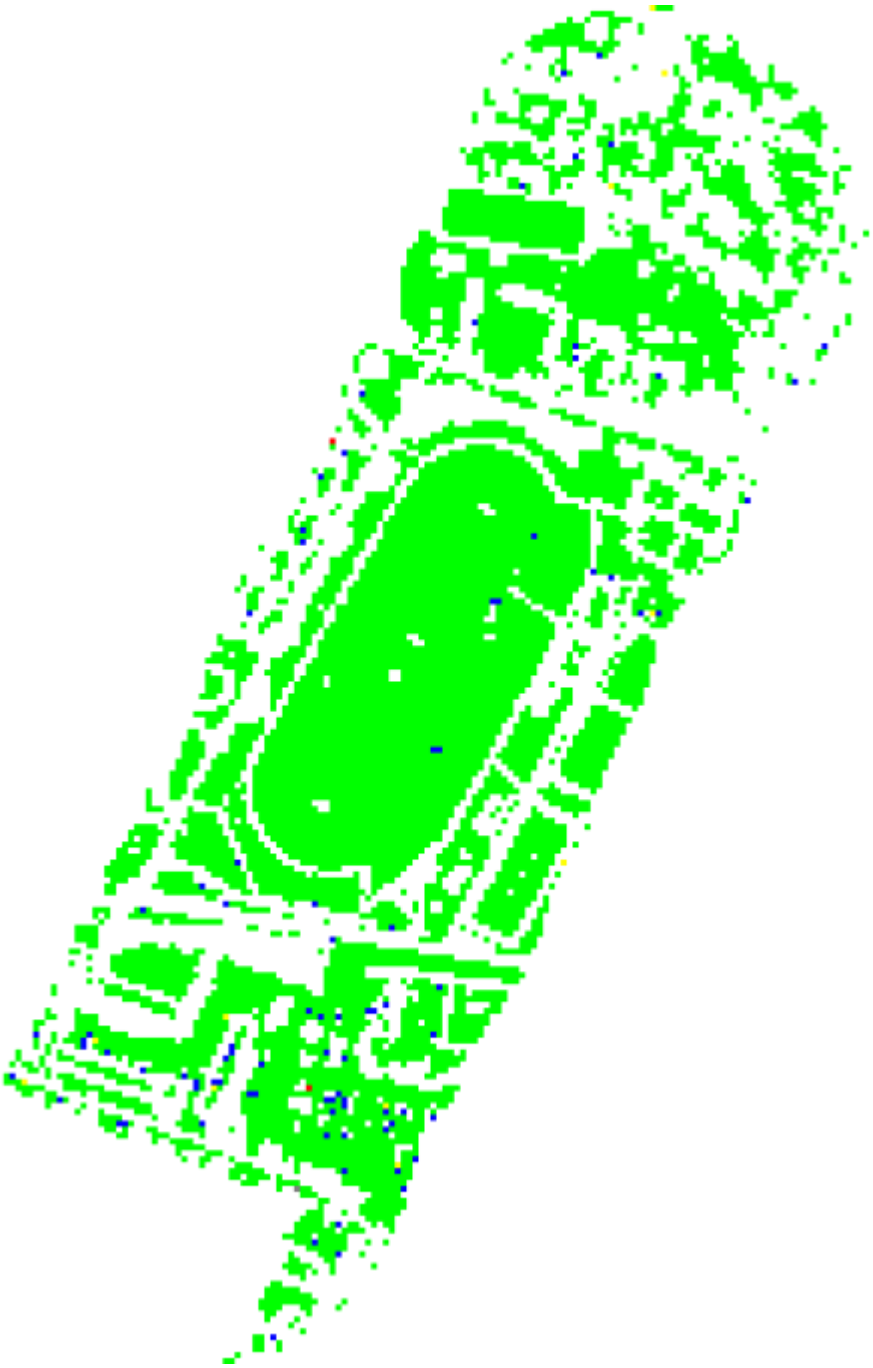

Flightline Accuracy Report Output:
ID003 Flightline 004 Shallow vs. ID008 Flightline 002 Shallow FL Accuracy

Limits	Patch#	First FL Positive	Average Error	Percentage
0.00 <= ERR <0.10	7913	54.93%	0.0126	98.74%
0.10 <= ERR <0.20	87	49.43%	0.1343	1.09%
0.20 <= ERR <0.30	11	81.82%	0.2471	0.14%
0.30 <= ERR <0.50	2	50.00%	0.3120	0.02%
0.50 <= ERR < Inf.	1	100.00%	0.5226	0.01%
Summery	8014	54.92%	0.0144	

Accuracy Index: 99

Patch Statistics
All#: 35037 | Valid: 25.15% | NumHit.fail:50.59% | Condist.fail:0.83% | Normalz.fail:18.47% | RMS.fail:4.95%

Scan accuracy, flightline 2:

Scan Accuracy Report Output:
ID008 Flightline 002 shallow Scan Accuracy

Limits	Patch#	Front Scan Positive	Average Error	Percentage
0.00 <= ERR <0.10	7140	20.49%	0.0166	97.98%
0.10 <= ERR <0.20	116	31.90%	0.1342	1.59%
0.20 <= ERR <0.30	21	28.57%	0.2337	0.29%
0.30 <= ERR <0.50	8	0.00%	0.3589	0.11%
0.50 <= ERR < Inf.	2	100.00%	1.3212	0.03%
Summary	7287	20.69%	0.0198	

Accuracy Index: 99

Patch Statistics
All#: 42237 | Valid: 19.00% | NumHit.fail:62.76% | ConDist.fail:0.79% | Normalz.fail:14.28% | RMS.fail:3.17%

6.2 Comparison between first and second calibration flight

Topo, flightline accuracy

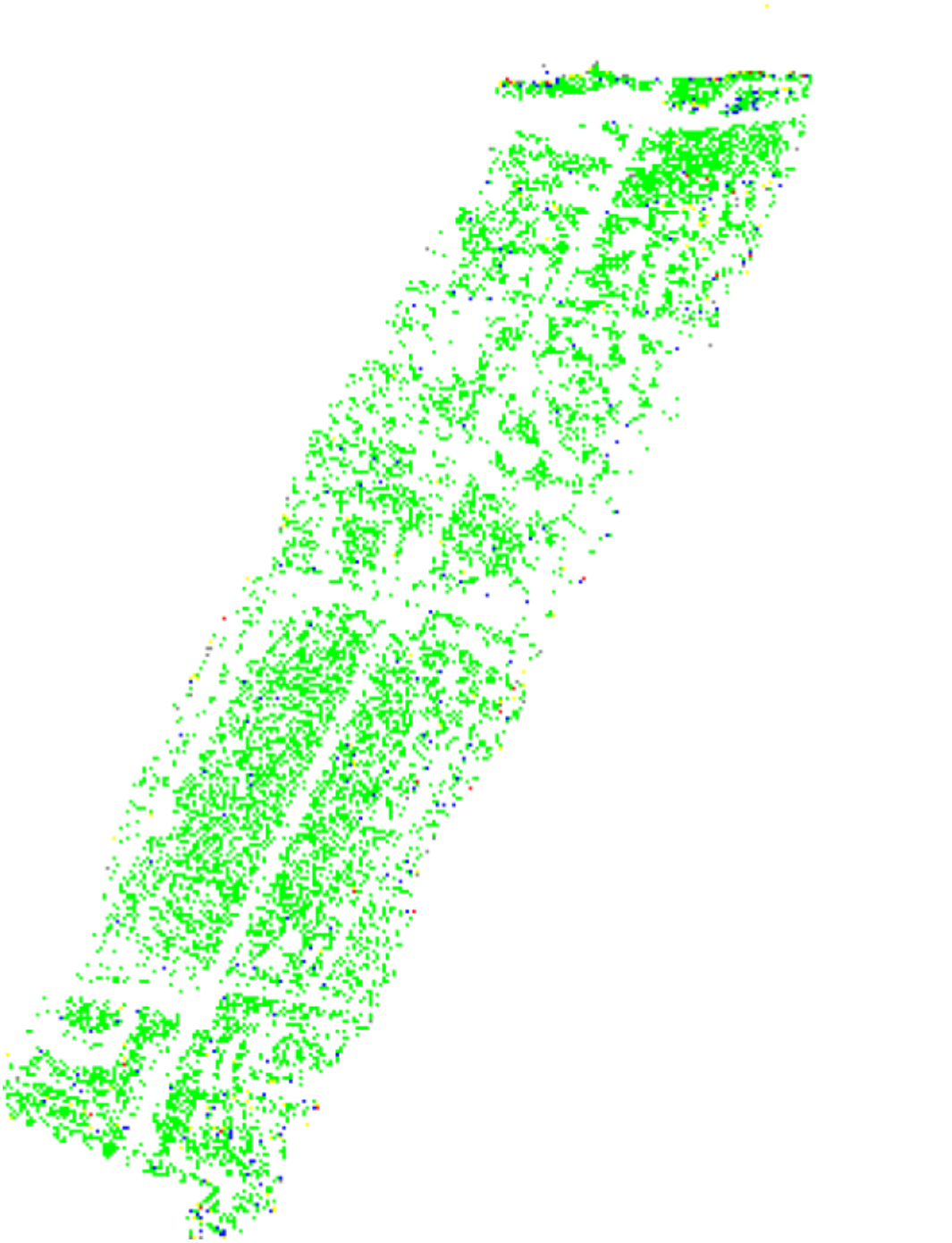

Flightline Accuracy Report Output:
ID003 Flightline 004 Topo 1 vs. ID005 Flightline 004 Topo 1 FL Accuracy

Limits	Patch#	First FL Positive	Average Error	Percentage
0.00 <= ERR <0.03	7921	32.37%	0.0073	95.16%
0.03 <= ERR <0.05	210	50.95%	0.0378	2.52%
0.05 <= ERR <0.10	122	48.36%	0.0673	1.47%
0.10 <= ERR <0.15	25	52.00%	0.1216	0.30%
0.15 <= ERR < Inf.	46	50.00%	0.3543	0.55%
Summery	8324	33.23%	0.0112	

Accuracy Index: 98

Patch Statistics
All#: 90768 | Valid: 15.18% | NumHit.fail:59.84% | Condist.fail:0.27% | Normalz.fail:11.01% | RMS.fail:13.70%

Hydro, flightline accuracy

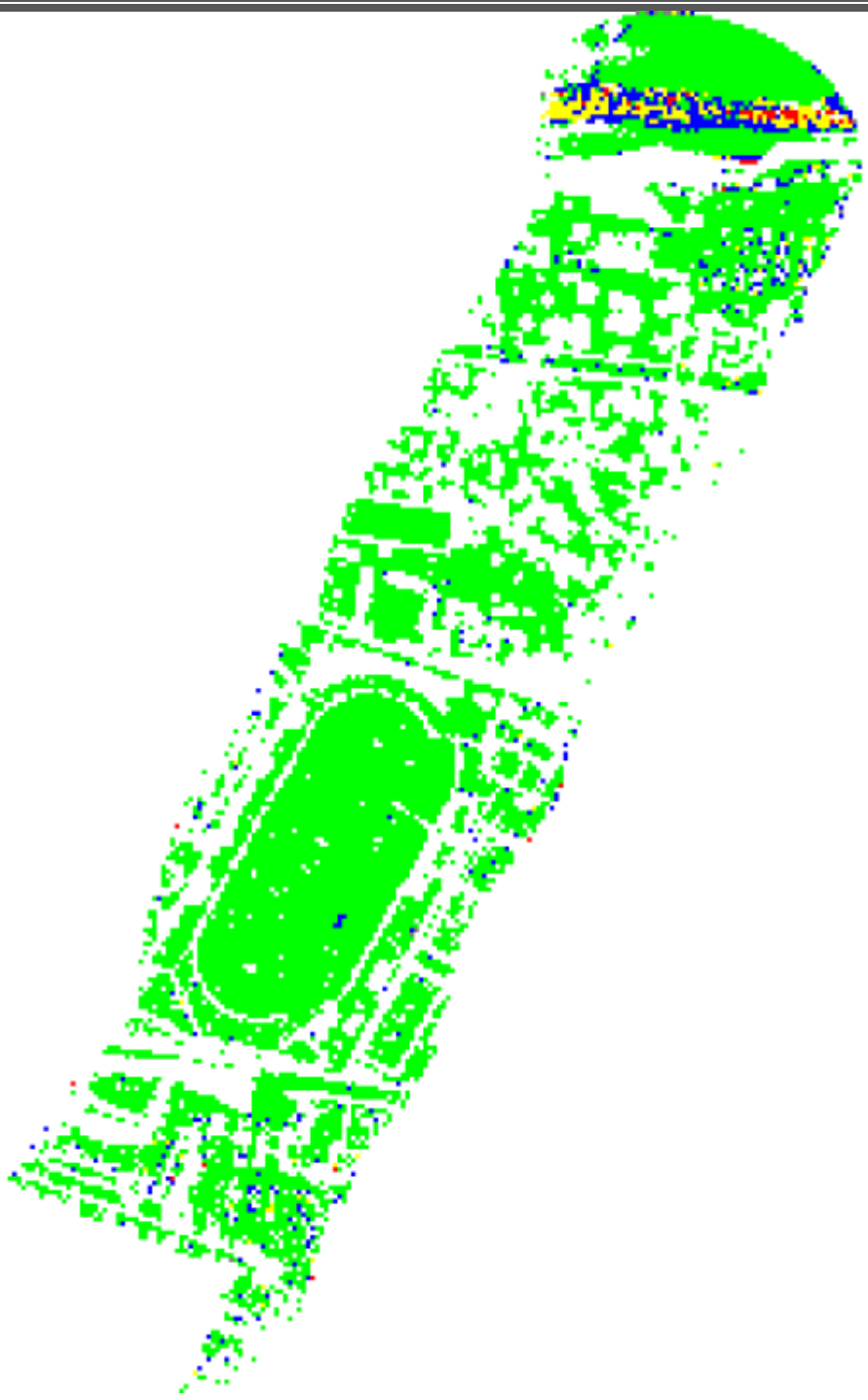

Flightline Accuracy Report Output:
ID003 Flightline 004 shallow vs. ID005 Flightline 004 shallow FL Accuracy

Limits	Patch#	First FL Positive	Average Error	Percentage
0.00 <= ERR <0.10	10195	74.44%	0.0208	92.65%
0.10 <= ERR <0.20	514	85.99%	0.1415	4.67%
0.20 <= ERR <0.30	232	95.69%	0.2395	2.11%
0.30 <= ERR <0.50	49	93.88%	0.3457	0.45%
0.50 <= ERR < Inf.	14	50.00%	0.7939	0.13%
Summery	11004	75.48%	0.0335	

Accuracy Index: 97

Patch Statistics
All#: 59976 | Valid: 25.18% | Numhit.fail:59.96% | Condist.fail:0.77% | Normalz.fail:8.72% | RMS.fail:5.36%

6.3 Comparison with reference points

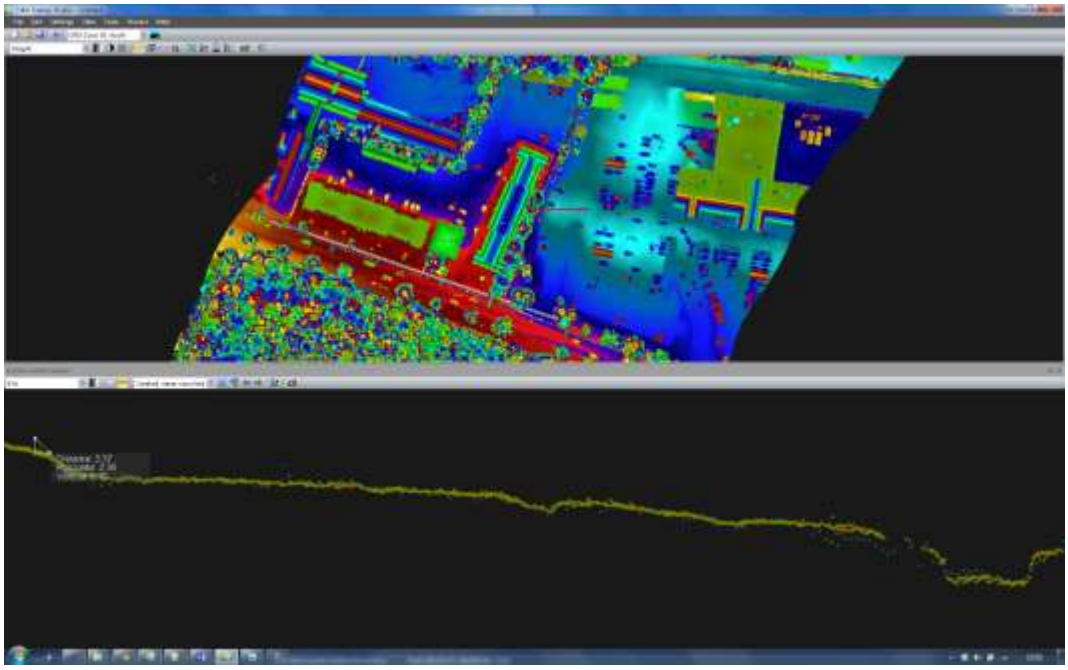

The image above shows one line from each laser, green is from the bathymetric laser, yellow from the topographic. Red are RTK reference points. Ruler inserted for scale.